Nanoscale Horizons

REVIEW

View Article Online
View Journal

Cite this: DOI: 10.1039/c8nh00274f

Recent advances in functionalized MnO_2 nanosheets for biosensing and biomedicine applications

Juan Chen,[a] Hongmin Meng,[a] Yuan Tian,[a] Ran Yang,[a] Dan Du,[b] Zhaohui Li, *[a] Lingbo Qu*[a] and Yuehe Lin *[b]

Received 30th August 2018,
Accepted 12th November 2018

DOI: 10.1039/c8nh00274f

rsc.li/nanoscale-horizons

As one kind of redox active layered transition-metal dioxide nanomaterials, single-layer manganese dioxide (MnO_2) nanosheets have gained significant research attention in the fields of biosensing and biomedicine because of their large surface area, intense and broad optical absorption, strong oxidation ability, catalytic activity, and robust mechanical properties. This review provides a brief overview of the recent advances in the development of MnO_2 nanosheet-based biosensors, bioimaging as well as drug delivery for cancer therapy. The methodologies for the preparation of MnO_2 nanosheets are summarized, followed by an introduction of the nanostructure and properties of MnO_2 nanosheets. Special attention is paid to their applications in biosensing, bioimaging and cancer therapy. Future perspectives and the challenges of high-performance MnO_2 nanosheets are also discussed.

Introduction

There are increasing demands for nanobiotechnology in various applications, such as biosensing, bioanalysis, bioimaging, and biomedicine, which have substantially promoted the development of a variety of nanosystems. One of the key issues in biomaterial development at the nanoscale is to the exploration of advanced functional nanomaterials with high performance. As a newly emerging class of nanomaterials, two-dimensional (2D) nanosheets, especially a wide variety of transition-metal oxide nanosheets with planar topography such as manganese dioxide (MnO_2), molybdenum disulfide (MOS_2) and cobaltosic oxide (Co_3O_4), exhibit unique properties including high specific surface area (SSA) and robust physicochemical properties. Furthermore, they are degradable and easy to modify, which makes them very promising nanoplatforms for biomedical applications.[1–4]

MnO_2 nanosheets are redox active 2D nanomaterials with thickness on the nanometer scale or even smaller, while the

[a] Henan Joint International Research Laboratory of Green Construction of Functional Molecules and Their Bioanalytical Applications, College of Chemistry and Molecular Engineering, Zhengzhou University, Zhengzhou 450001, P. R. China. E-mail: zhaohui.li@zzu.edu.cn, qulingbo@zzu.edu.cn
[b] School of Mechanical and Materials Engineering, Washington State University, Pullman, WA 99164, USA. E-mail: yuehe.lin@wsu.edu

Juan Chen

Juan Chen received her Master's degree in Chemistry from Nanchang University in 2016. She has been pursuing her PhD degree at the College of Chemistry and Molecular Engineering at Zhengzhou University since 2016, and her main research interests are in nanomaterials-based chemo/bioassays.

Hongmin Meng

Hong-Min Meng received her BS in 2010 and PhD in 2015, both from the Department of Chemistry, Hunan University. She has been an Assistant Professor in the College of Chemistry and Molecular Engineering at Zhengzhou University since 2017. Her research interests include constructing novel functional nucleic acid-conjugated nanostructures for bioassays, bioimaging and drug delivery.

lateral size ranges from sub-micrometers to micrometers.[5,6] The MnO_2 nanosheets have three atomic layers, *i.e.*, one Mn layer sandwiched by two O layers.[7] Each Mn coordinates to six O atoms to form edge-sharing MnO_6 octahedra. The existence of Mn-vacancies makes MnO_2 nanosheets negatively charged and repulsive to each other.[8] Moreover, the d–d transitions of Mn ions in the MnO_6 octahedra of MnO_2 nanosheets result in a broad absorption spectrum ($\sim$200–600 nm) with a large molar extinction coefficient (ε_{max} = 9.6 $\times$ 10^3 M^{-1} cm^{-1}) at 380 nm.[6]

The properties of nanomaterials are largely affected by their structures. The special features MnO_2 nanomaterials and the corresponding applications are summarized as follows: (1) due to the edge-shared octahedral crystal structure and the large surface area, the layered MnO_2 possesses good absorption and degradation ability toward different kinds of organic pollutants, dyes and heavy metal ions, which makes it an environmental-friendly material.[9–11] (2) The broad absorption spectrum of MnO_2 nanosheets overlaps with the fluorescence excitation and/or emission spectra of most kinds of organic dyes, quantum dots, fluorescence nanoparticles and metal nanoclusters, which endows MnO_2 nanosheets with strong fluorescence quenching ability.[12–15] Based on this property, Förster resonance energy transfer (FRET) and the inner filter effect (IFE) can occur between MnO_2 nanosheets and the organic dyes/fluorescence nanomaterials.[8] (3) MnO_2 platelets can adsorb single-stranded DNA (ssDNA) through van der Waals forces between nucleobases and the basal plane of MnO_2 platelets, while releasing double-stranded DNA (dsDNA) because of their negative charge, so it has often been used as a new class of biosensing platform for probing DNA hybridization and aptamer–target interactions in a homogeneous solution.[16] (4) The valence state of Mn^{4+} in MnO_2 is the intermediate valence, so the MnO_2 nanosheets themselves have strong oxidation ability and catalytic activity, which can be rapidly degraded by some redox reactions with reducing substances. In the presence of a reducing substance (taking GSH as an example), MnO_2 can be reduced to Mn^{2+}, leading to the decomposition of the MnO_2 nanosheets, as shown in eqn (1).

$$2GSH + MnO_2 + 2H^+ \rightarrow GSSG + Mn^{2+} + 2H_2O \quad (1)$$

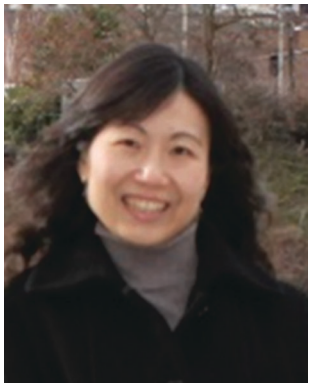

Dan Du

Dan Du received her PhD in Analytical Chemistry from Nanjing University in 2005. She joined Central China Normal University in 2005 and was promoted to Full Professor in 2011. Currently she is a Research Professor at Washington State University. Her research interests include functional nanomaterials for biosensing and drug delivery. She has published over 250 papers, with citations of 10 600, h-index 60.

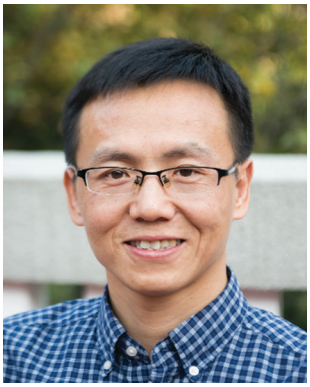

Zhaohui Li

Zhaohui Li received his PhD degree at the State Key Laboratory of Chemo/Biosensing and Chemometrics at Hunan University in 2007. He did his postdoctoral training in the Walt Group at Tufts University from 2007 to 2009 and in the Pacific Northwest National Laboratory from 2009 to 2011. At present, he is a full Professor at Zhengzhou University. His research interests are mainly focused on nanomaterial preparation and their applications in chemo/biosensing.

Lingbo Qu

Lingbo Qu received his PhD degree in Pharmaceutical Analysis at China Pharmaceutical University in 1997. He did his postdoctoral training at the Pharmaceutical Institute at Peking Union Medical College from 1997 to 1999. At present, he is a full Professor at Zhengzhou University. His research interests are mainly focused on drug molecule design and drug analysis.

Yuehe Lin

Yuehe Lin is a Professor at Washington State University and a Laboratory Fellow at Pacific Northwest National Laboratory. His research interests include electrochemistry, bioanalytical chemistry, chemical sensors and biosensors, nanomaterial synthesis and applications. He has over 20 patents and has published about 450 papers, with a total citation of 45 000, H-index 110. He was elected to the Washington State Academy of Sciences in 2018. He is a fellow of the American Association of the Advancement of Science (AAAS), the Royal Society of Chemistry (RSC), and the American Institute for Medical and Biological Engineering (AIMBE).

Therefore, MnO_2 nanosheets have been used as oxidants to detect reducing substances in biological samples.[17,18] In addition, Mn^{2+} has been used in MRI contrast agents for bioimaging. (5) With a large specific surface area and high drug-loading amount, recent studies have shown that MnO_2 nanosheets as nanocarriers can penetrate across the cell membrane and have been widely used for drug delivery and cancer therapy.[19,20]

Due to the unique properties of MnO_2 nanosheets, they have been widely used to construct nanosystems for biomedical applications including biosensing,[21–24] drug delivery,[25] bioimaging,[26] and cancer therapy.[27] (Fig. 1). A review article on this topic is timely, as a large number of studies are being reported on both chemical and biological sensors using MnO_2 nanosheets and their growing commercial attention.[28] Besides, varied methods have achieved great success in the preparation of MnO_2-based materials with different nanostructures. However, a comprehensive summary of techniques developed for synthesizing MnO_2 nanosheets has not yet been reported. In this feature article, we shed light on the recent developments in synthesizing MnO_2 nanosheets and their applications in biosensing, bioimaging, and drug delivery. The remaining challenges and future prospects of MnO_2 nanosheets will also be highlighted and discussed.

Synthesis of MnO_2 nanosheets

There are two major approaches to preparing MnO_2 nanosheets: the top-down approach and the bottom-up approach. As shown in Fig. 2A, the top-down approach for the synthesis of MnO_2 nanosheets requires a multistep process: (1) a high-temperature solid-state reaction (to yield a thermodynamically stable precursor phase, *e.g.*, K/MnO_2); (2) protonation of interlayer alkali metal ions (to yield, *e.g.*, H/MnO_2), and (3) an acid–base reaction with an aqueous solution of quaternary ammonium cations (to finally yield negatively charged nanosheets, *e.g.*, MnO_2 in the form of a colloidal suspension).[5,29] This approach is costly and time-consuming. Moreover, it is fairly difficult to exfoliate the protonated compounds into single-layer nanosheets, resulting in the wide thickness distribution of the final products. Herein, we mainly discuss the bottom-up approach.

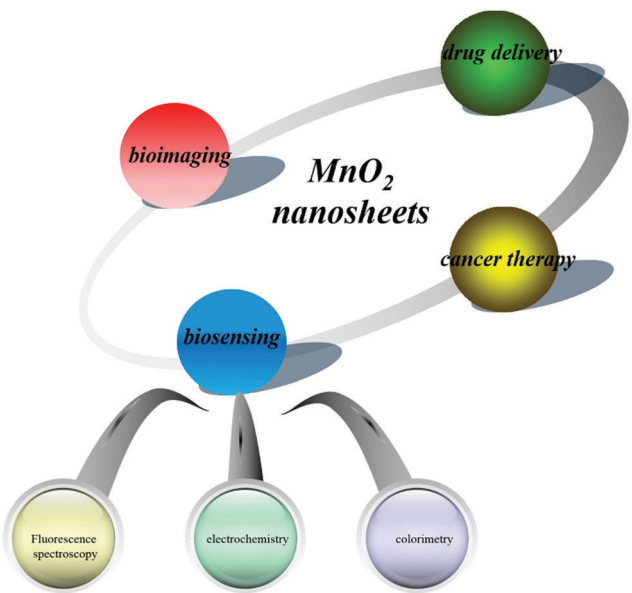

Fig. 1 Schematic illustration of MnO_2 nanosheets for applications in biosensing, bioimaging, drug delivery and cancer therapy.

In 2007, Oaki and Imai[30] reported for the first time the one-pot bottom-up synthesis of MnO_2 nanosheets in aqueous solution without the requirement of high-temperature hydrothermal treatment and special equipment. The authors employed ethylenediaminetetraacetate (EDTA) as the chelating agent for Mn^{2+} ions so as to inhibit the rapid precipitation of $Mn(OH)_2$. However, the obtained materials were in the multilayer structure rather than a monosheet, and the whole process required 3–5 days. On this basis, Kawamata *et al.*[6] successfully demonstrated the first single-step approach to access the MnO_2 nanosheets directly within one day. So far, this simple single-step approach has attracted tremendous attention, and a number of broad new studies on further developing MnO_2 nanocomposites based on this approach have emerged. Moreover, this high-yield simple route to synthesizing the MnO_2 monosheets within a day has been developed to construct a unique structure (Fig. 2B–D) by different improved methods such as the hard template method, soft template method and template-free method.

Hard template method

Hard templates are those materials that are used as scaffolds for the nanomaterial deposition or employed as the nucleus coated by the desired nanomaterials. The main hard template approach uses a simple hydrothermal method for deposition without any surfactants. For the deposition of MnO_2 nanomaterials, $KMnO_4$ was used in the hydrothermal reaction as the Mn precursor. After several hours of hydrothermal reaction, MnO_2 nanosheets were formed on the surface of the hard templates, including graphene oxide (GO),[31] montmorillonite K10,[24] silica nanoparticles (SiO_2 NPs),[32] ferroferric oxide nanoparticles (Fe_3O_4 NPs),[33] and so on.

For example, Feng *et al.*[31] proposed a hydrothermal method to prepare MnO_2/graphene nanocomposites. As we know, on the surface and edge of GO, there are a lot of functional groups, *e.g.*, ketone, quinine, carboxylic, hydroxyl, *etc.*, which make GO negatively charged. Thus, upon the addition of $MnSO_4$ to the GO suspension, Mn^{2+} can be attached to the graphene surfaces through the electrostatic effect. After the addition of the oxidant $KMnO_4$, lots of MnO_2 nuclei were immediately formed on the surface of GO due to the redox reaction between the Mn^{2+} and MnO_4^-. Then, with the process of hydrothermal reaction at 140 °C for 2 h, GO was reduced and MnO_2 nanosheets were successfully prepared. The different morphologies of the final composites were controlled by the amount of Mn^{2+} source.

Using a similar strategy, MnO_2 nanosheets on montmorillonite (MnO_2 nanosheets@MMt) were synthesized by a one-pot method.[24] Montmorillonite K 10 was added to a $KMnO_4$

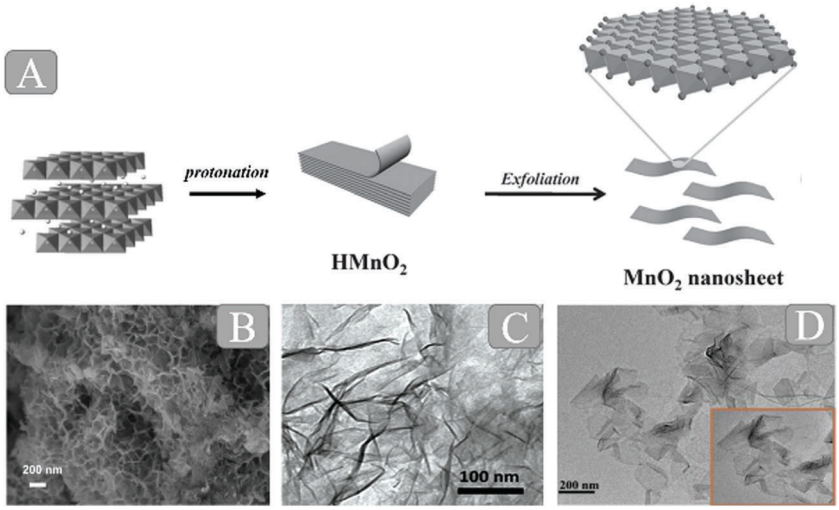

Fig. 2 (A) Schematic illustration of the synthetic procedure for 2D MnO_2 nanosheets. Reprinted with permission from ref. 99. Copyright (2014) Wiley-VCH. (B) SEM images of the MnO_2 nanosheets based on the hard template method. Adapted with permission from ref. 24. Copyright (2018) Elsevier. (C) TEM image of MnO_2 nanosheets based on the soft template method. Reprinted with permission from ref. 36. Copyright (2015) Wiley-VCH. (D) HRTEM images of MnO_2 nanosheets based on the free template method. Adapted with permission from ref. 96. Copyright (2017) American Chemical Society.

solution without any surfactants and then subjected to stirring and ultrasonic treatment at room temperature. The mixture was added to a Teflon-lined stainless steel autoclave and maintained at 160 °C for 24 h. After that, the honeycomb-like MnO_2@MMt was obtained. Compared with the montmorillonite, the MnO_2 nanosheets@MMt showed high adsorption capacity of 363.63 mg g^{-1} for MB dye and can improve adsorption performance and redox reactivity for organic pollutants. The morphology of MnO_2 nanostructures can be adjusted by changing the reaction time, annealing process or the amount of reducing agents.

In summary, hard template methods can be used for the controlled synthesis of ordered MnO_2 nanostructures through the hydrothermal reaction. Moreover, because no surface active agents are involved, the interference of other substances during the formation of MnO_2 is effectively reduced. However, these hard template methods often require high temperature, high pressure, and long reaction time. Therefore, the development of low-cost and simple templating methods for fabricating unique MnO_2 nanostructures it is desired.

Soft template method

The soft template method is also applied in the synthesis of MnO_2 nanostructures. Soft templates include surfactants,[16,34] flexible organic molecules,[20] bioprotein[35] or block copolymers,[26] all of which can act as structure-directing agents in the formation of MnO_2. During the process of synthesizing MnO_2 nanostructures, micelles have different morphologies depending on the different surfactant concentrations. Taking the electrostatic attraction, hydrogen bonding and van der Waals forces between surfactant molecules and nanomaterials as driving forces, these special micellar structures are used to effectively guide the precursors of the free nanomaterials to synthesize designed nanostructures.

Using sodium dodecyl sulfate (SDS) as the template (Fig. 3), colloidal MnO_2 nanosheets were synthesized in one step.[36] Gu *et al.* synthesized single-layer MnO_2 nanosheets *via* a redox reaction between $KMnO_4$ and SDS under acidic condition. The gradual hydrolysis of SDS was found to be the key factor for the successful formation of single-layer nanosheets. SDS serves not only as the precursor of dodecanol to reduce $KMnO_4$ but also as a structure-inducing agent to aid the formation of single-layer MnO_2 nanosheets. Zou *et al.*[16] employed cetyltrimethylammonium bromide (CTAB) as the cationic surfactant template, 2-(*N*-morpholino)ethanesulfonic acid (MES) as the reducing agent and $KMnO_4$ as the Mn precursor to prepare the water-dispersed nano-MnO_2 materials at room temperature. Such a template can self-assemble into a stable supramolecular structure (oil/water emulsion) in aqueous solution; the redox reaction between $KMnO_4$ and MES quickly occurred at the oil/water interface and produced MnO_2 nuclei *in situ*.[37] These MnO_2 nuclei continually grew into nano-MnO_2 materials, and thus an unstable shell of loosely packed platelets was formed. After removing CTAB and other residual reactants, the shell collapsed, yielding the purified nano-MnO_2 materials.

With the development of the bio-template synthesis method, the protein-directed *in situ* synthesis of nanomaterials has received a lot of attention due to the cost-effective, simple and environmentally friendly synthesis process. Most of the reported protein-templated nanomaterials show the morphologies of nanosheets (NSs),[38] nanoparticles (NPs)[39] and nanoclusters (NCs),[40] and it is worth mentioning here that Liu *et al.*[35] employed the capsid proteins pVIII of phage M13 as bio-templates to synthesize MnO_2 nanosheets for the first time. MnO_2 nanosheets were synthesized by the spontaneous oxidation of Mn^{2+} in an alkaline solution containing pVIII in the air at room temperature. Although the detailed mechanism is not clear and remains to be further investigated, the as-prepared protein–MnO_2 nanosheets have

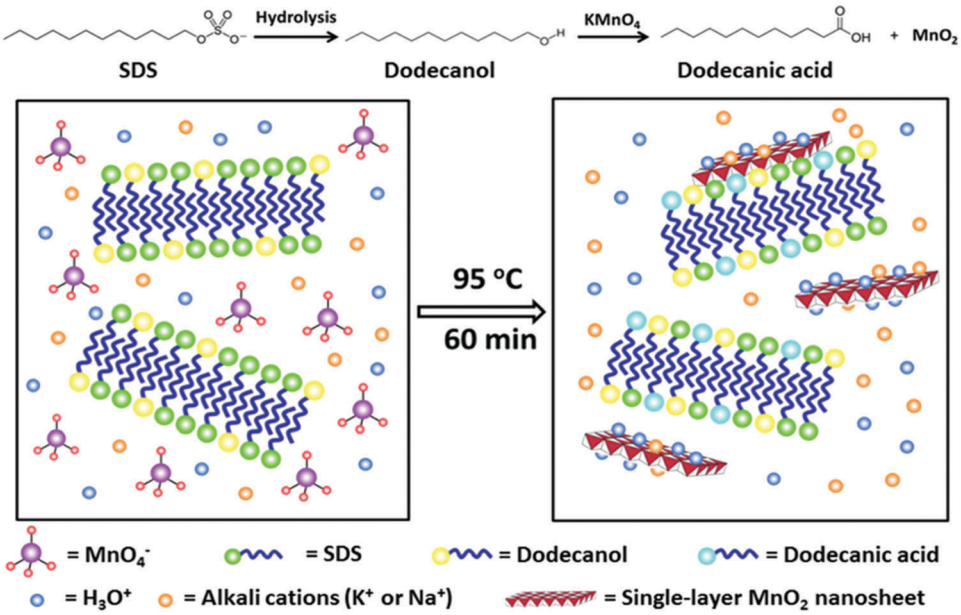

Fig. 3 Schematic illustration of the lauric acid and SDS co-modified MnO_2 nanosheets formation by *in situ* redox reaction between $KMnO_4$ and dodecanol on the surface of the preformed soft-template. Reprinted with permission from ref. 36. Copyright (2015) Wiley-VCH.

shown intrinsic peroxidase-like activity and excellent antioxidant behaviors of natural antioxidants.

Although conceptually simple and versatile, the soft template method has its own limitations. This method often has difficulty in controlling the size, shape and uniformity of the products. Besides, the residual surfactants, organic substances and macromolecules may increase the ion resistance, proteins as bio-templates may be expensive, and the template removing process is time-consuming. Therefore, there still remains a major challenge to develop a facile, low cost, and environmentally benign method for the controllable synthesis of MnO_2 materials.

Free template method

Apart from the abovementioned template-assisted methods, there are many other techniques that can be used to synthesize MnO_2 nanosheets in the absence of an additional template. By employing $MnCl_2{\cdot}4H_2O$ as the Mn precursor and H_2O_2 as the oxidizing agent, Kawamata *et al.*[6] successfully demonstrated the free template approach to directly form the MnO_2 nanosheets within a day. In the presence of hydrogen peroxide (H_2O_2) and tetramethylammonium cations (TMA), Mn^{2+} ions were oxidized to MnO_2 in an aqueous solution at room temperature. The cation not only served to inhibit the flocculation of the monosheets but also to exfoliate the locally aggregated monosheets in the suspension. The obtained monolayer MnO_2 nanosheets possess good dispersibility and are not easily agglomerated. The reports on using this method to synthesize MnO_2 nanosheets are springing up.

Using this typical synthesis, Xie[41] demonstrated experimentally that the chemical introduction of double-exchange in MnO_2 nanosheets brought a metal–insulator transition near room-temperature. First, the bulk 2D MnO_2 was prepared by adding $MnCl_2{\cdot}4H_2O$ into the $(NH_4)_2S_2O_8$ and TMA (25 wt%) solution under vigorous stirring for 60 min. The pristine MnO_2 nanosheet was obtained by adding the bulk 2D MnO_2 nanosheet to the water for ultrasonic treatment under constant temperature at 25 °C. The treated MnO_2 nanosheet was obtained from the pristine MnO_2 nanosheet by heating at 100 °C for 30 min and then at 220 °C for 2 h in a N_2 atmosphere. The obtained films were characterized by X-ray diffraction (XRD), high-resolution transmission electron microscopy (HRTEM), atomic-force microscopy (AFM) and X-ray photoelectron spectra (XPS). The double-exchange Mn(III)–O–Mn(IV) structure was confirmed to be successfully produced by a low-oxygen-pressure thermoannealing of pristine MnO_2 nanosheets (Fig. 4). The rapid development of nanoscience and technology has brought change to the MnO_2 preparation technique and a few materials and more convenient methods are being used to prepare MnO_2 nanosheets. The MnO_2 nanomaterials can be fabricated by a facile one-step redox method by the addition of aqueous $KMnO_4$ as the Mn precursor in the presence of 2-(*N*-morpholino)-ethanesulfonic acid (MES) buffer at pH 6.0. $KMnO_4$ was sonication-induced for 30 min directly and reduced by MES to form MnO_2 nanosheets at room temperature. This method has received considerable attention for preparing MnO_2 nanosheets due to the significant advantages such as less interfering substances, simple formation process and short preparation time. However, the prepared MnO_2 nanosheets were thick, agglomerated easily, and unstable.

An even more relevant reason is as follows: in the presence of a fluorescence reporter (*e.g.* CQDs), the addition of $KMnO_4$ and MES can generate MnO_2–CQDs nanocomposites *in situ*, and simultaneously quench the fluorescence of the labels, which can reduce the tedious steps and material interference in the formation of a fluorescence quenching system. For instance, Deng *et al.*[21] used a template-free method to direct the growth

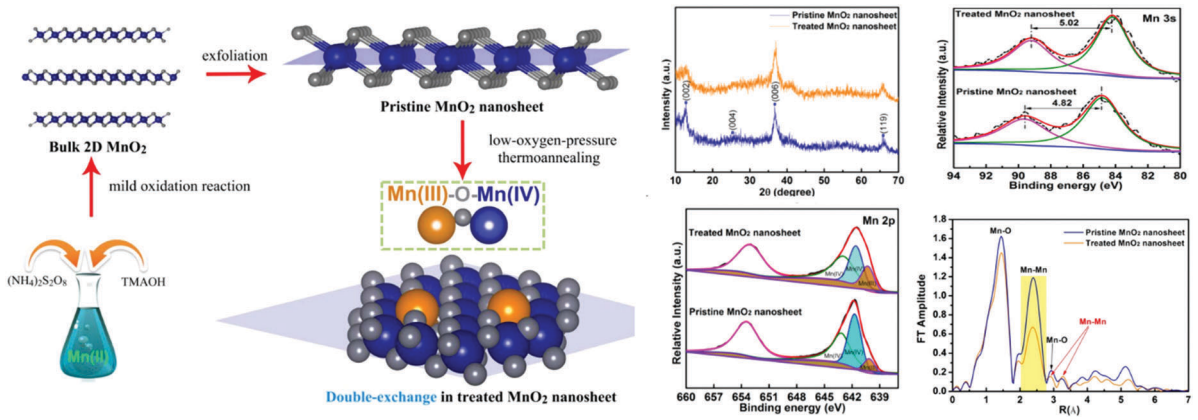

Fig. 4 Schematic illustration of the synthesis strategy for the 2D MnO_2 nanosheet with Mn(III)–O–Mn(IV) double-exchange structure, and investigation of the systematic characterization. Adapted with permission from ref. 41. Copyright (2017) American Chemical Society.

of MnO_2 nanosheets on the surface of the core–shell $NaYF_4$:Yb/Tm@$NaYF_4$ nanoparticles in the presence of $KMnO_4$ and MES buffer. Subsequently, various MnO_2 nanostructures have been synthesized by a template-free method with different labels.[42–44] In the recent study by Chen *et al.*,[17] the graphitic-phase C_3N_4 (g-C_3N_4) nanosheet–MnO_2 sandwich nanocomposite was fabricated by a facile one-step *in situ* approach for the first time. The as-prepared MnO_2 nanoparticles have a broad absorption band from 250 to 500 nm, which matches well with the reported optical characteristics of MnO_2 nanomaterials.[45] Remarkably, the absorbance spectrum of MnO_2 nanoparticles overlaps well with the fluorescence emission of the g-C_3N_4 nanosheet, thereby leading to fluorescence resonance energy transfer (FRET) from the g-C_3N_4 nanosheet to the MnO_2.

Biomedical applications of MnO_2 nanosheets

The unique 2D planar structure and the above-mentioned series of characteristics have led to unique properties of MnO_2 nanosheets for biomedical applications. To date, MnO_2 nanosheets have been explored for a variety of biomedical applications such as sensing, molecular adsorption, biological imaging, drug delivery and cancer therapy. In addition, the biological effect and behavior of MnO_2 nanosheets are also now under extensive exploration. It has been demonstrated that MnO_2 nanosheets present low cytotoxicity and high hemo-/histo-compatibility. In this section, we mainly summarize the biomedical applications of MnO_2 nanosheets in biosensing, imaging and cancer therapy.

MnO_2 nanosheet-based biosensor

Based on the oxidizing ability and catalytic activity of MnO_2, MnO_2 nanosheets have been widely used to construct biosensors. These biosensors can be mainly classified into three types: fluorescence biosensors, electrochemical biosensors and colorimetric biosensors.

MnO_2 nanosheet-based fluorescence biosensors

MnO_2 nanosheets are generally used as fluorescence quenchers in fluorescence assays due to their strong optical absorption and fast electron transfer. MnO_2 has been widely used for the detection of reducing substances due to its selective decomposition of MnO_2 to Mn^{2+} ions. The fluorescence of the fluorescent materials is initially quenched by the MnO_2 nanosheets. When in the presence of reducing target substances, the reductive reactions take place between the target and MnO_2 nanosheets, and the MnO_2 nanosheets are reduced to Mn^{2+} ions. As a result, the fluorescent labels are released and the fluorescence is recovered with the intensity directly related to the concentration of the target. By coupling with different kinds of fluorescent nanomaterials, many reducing substances can be detected based on this principle. GSH is a thiol-containing tripeptide that is generally treated as an essential endogenous antioxidant in cellular defense against toxins and free radicals.

Deng *et al.*,[21] for the first time, reported a MnO_2-UCNPs based nanoprobe for GSH detection. In this nanosystem, the fluorescence of UCNPs (up-converting nanoparticles) can be effectively quenched by wrapping the MnO_2 nanosheets on the surface of UCNPs. When the GSH was added to the solution, the fluorescence was restored due to the reductive reactions between the GSH and MnO_2 nanosheets. The principle of a designed assay was demonstrated in Fig. 5A. By monitoring the fluorescence signal change of UCNPs, GSH in aqueous solutions and cancer cells can be detected. A limit of detection of 0.9 mM was achieved for GSH detection. Based on this principle, various fluorescence nanomaterial-MnO_2 assays, such as carbon dot–MnO_2 nanosheets,[14,46–55] quantum dot–MnO_2 nanosheets,[34,56–59] organic dye–MnO_2 nanosheets,[8,60–63] metal nanocluster–MnO_2 nanosheets,[43,64,65] and polymer fluorescence nanoparticles,[13,66–70] were developed for the detection of GSH and other reductive substances.

Our group[14] also reported a facile one-step approach for the rapid and selective sensing of GSH based on the fluorescence resonance energy transfer (FRET) of C-dots–MnO_2 nanocomposites (Fig. 5B). Soon after, a large amount of work about CQDs and MnO_2 complexes for the detection of different reductive substances was reported. For example, Lin *et al.*[54] and Zou *et al.*[53] reported a novel FRET-based sensing platform using fluorescent C-dots and MnO_2 nanosheets as the energy donor–acceptor

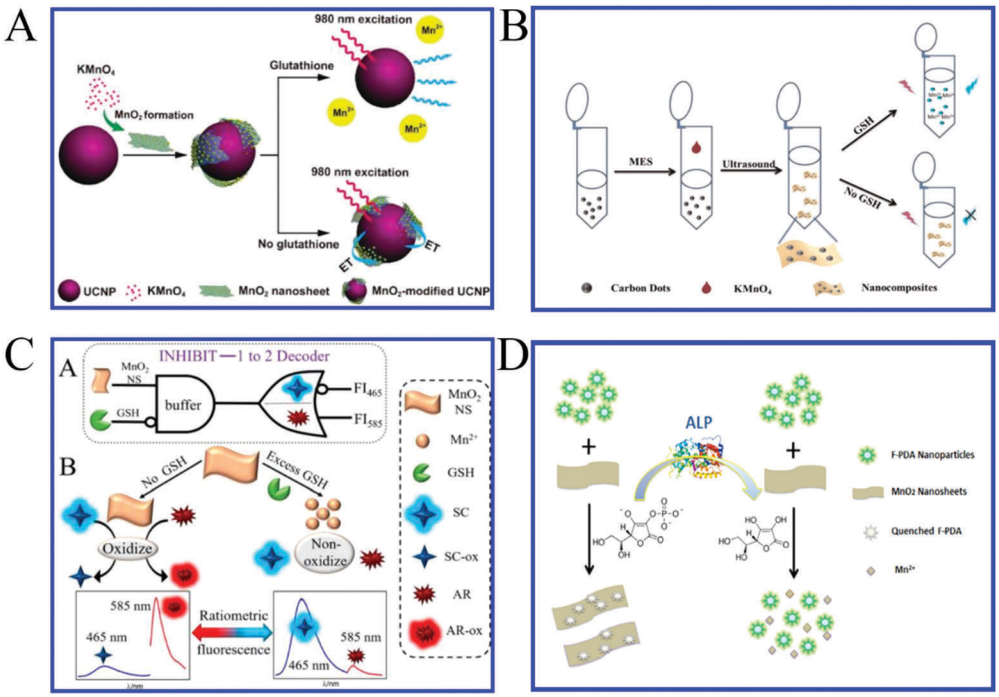

Fig. 5 (A) Experimental design for GSH detection using MnO_2-nanosheet-modified upconversion nanoparticles. Adapted with permission from ref. 21. Copyright (2011) American Chemical Society. (B) Schematic principle of C-dots–MnO_2 nanocomposites for GSH detection. Adapted with permission from ref. 14. Copyright (2015) Elsevier. (C) Illustration of the cascade logic circuit (INHIBIT-1 to 2 Decoder) and schematic operations of the MnO_2 NS-based ratiometric fluorescence sensor for GSH based on two fluorescent substrates. Adapted with permission from ref. 12. Copyright (2017) American Chemical Society. (D) Schematic illustration of the F-PDA–MnO_2 probe for ALP detection on the basis of FRET. Adapted with permission from ref. 66. Copyright (2018) American Chemical Society.

pairs for GSH sensing in human whole blood samples and intracellular fluid, respectively. To further explore the level of GSH in living cells, our group[56] developed a convenient fluorescence "turn-on" nanosensor based on graphene quantum dots (GQDs)–MnO_2 nanosheets for the selective detection of GSH in living cells. The limit of detection was 150 nM for GSH.

Generally, MnO_2 nanosheets are quenching agents, but Fan *et al.*[12] found that MnO_2 nanosheets can not only largely quench the fluorescence of highly fluorescent Scopoletin (SC) but also enhance that of nonfluorescent Amplex Red (AR) (Fig. 5C). Taking advantage of this property and the unique reaction between GSH and MnO_2 nanosheets, they constructed the first MnO_2 nanosheets-based ratiometric fluorescence sensor that is programmed for the ultrasensitive and selective detection of GSH by a cascade logic circuit. The calculated detection limit reached as low as 6.7 nM, which is the most sensitive MnO_2 nanosheets-based fluorescent GSH sensor reported so far.

Due to the convenience, quickness and high accuracy, point-of-care testing (POCT) will be the main force in clinical laboratory science in the future. It can be used directly in situations that have limited resources or medical facilities. The main prospects for using these fast POCT diagnostics include portability, user-friendliness, durability, cheapness and the ability to produce fast results. Among them, the most well-known POCT technique is the lateral flow test strip assay, whose unique advantage lies in speediness; it is also low cost, simple, and convenient. Our group developed a novel fluorescence lateral flow biosensor for GSH detection based on quantum dot–MnO_2 nanocomposites, which may have great potential to be used for GSH detection in point of care diagnosis.[58]

MnO_2 nanosheets can also be degraded by hydrogen peroxide (H_2O_2). Based on this principle, Wang[43] reported MnO_2 nanosheets–CuNC nanoprobes for the rapid and sensitive detection of H_2O_2 and glucose in human serum. In this design, the fluorescence of CuNCs (measured at excitation/emission wavelengths of 335/410 nm) was quenched when adding MnO_2 nanosheets into a colloidal solution of CuNCs. When H_2O_2 was added, MnO_2 nanosheets were degraded to restore the fluorescence of CuNCs. Thus, the detection of H_2O_2 was achieved. In addition, glucose is further detected based on the characteristics of glucose producing H_2O_2 under the action of its oxidase. Compared with the traditional methods of glucose detection, the strategy is convenient, low-cost and without a complicated procedure. Second, it is operated under mild conditions within several minutes. Third, it provides an alternative platform for detecting other substrates (*e.g.*, cholesterol) through oxidation by the O_2-dependent oxidase (*e.g.*, cholesterol oxidase), which can generate H_2O_2.

Ascorbic acid (AA), commonly known as vitamin C, is an antioxidant, an enzyme cofactor and essential nutritional factor in organisms. It can participate in hydroxylation and reduction reactions. It is also widely used in many fields, serving as an antioxidant in food, animal feed, beverages, cosmetics, and pharmaceutical formulations. A lack of AA in humans can

cause a variety of diseases, such as scurvy. Mao *et al.*[8] developed a new fluorescence method for the *in vivo* sensing of AA in the rat brain through suppressing the fluorescence of 7-hydroxycoumarin with the presence of MnO_2 nanosheets. The mechanism for the fluorescence suppression is attributed to a combination of the inner filter effect (IFE) and static quenching effect (SQE), which is different from those reported for the traditional two-dimensional nanosheets, and the Förster resonant energy transfer (FRET) mechanism reported for MnO_2 nanosheets. The limit of detection was estimated to be 8.7 ± 2.5 μM. This study not only offers a new avenue for *in vivo* sensing of AA but also provides new insight into MnO_2 nanosheets suppressing the fluorescence of dyes. In order to avoid the poor photostability of dyes, Yang *et al.*[66] recently reported a label-free, visual, reversible fluorescence biosensor for the convenient assaying of ALP activity based on the AA triggered reduction of MnO_2 nanosheets, as well as clarified the quenching mechanism of F-PDA nanoparticles by MnO_2 nanosheets (Fig. 5D).

Organophosphorus pesticides (OPs) are widely used in agricultural production because of their high efficacy and easy degradation in the environment. Because of their widespread use, organophosphorus pesticide residues in food and the environment have greatly threatened human health and caused widespread concern. Our group[50] developed a facile fluorescence platform for the sensitive detection of OPs based on single-layer MnO_2 nanosheets with C-dots as the signal readout. In the presence of butyrylcholinesterase (BChE) and acetylthiocholine, acetylthiocholine (ATCh) can be hydrolyzed to thiocholine by BChE; thiocholine reduced the MnO_2 nanosheets to Mn^{2+}. As a result of the decomposition of the MnO_2 nanosheets, the fluorescence of C-dots was recovered. OPs as an inhibitor to suppress BChE activity can decrease the decomposition of MnO_2, which again results in the fluorescence quenching. The fluorescence signal change corresponded to the degree of OPs-induced inhibition reaction. The linear detection range from 0.05 to 5 ng mL^{-1} was achieved for paraoxon detection with a limit of detection of 0.015 ng mL^{-1}. This sensing system provided a new method for probing another reducing agent product-related enzyme system. Beyond this, MnO_2 nanosheet-based DNA adsorption sensors are also very important. Layered transition-metal nanomaterials with one or a few atomic layers, recognized as planar covalent-network solids, have attracted growing attention in the past few years owing to their special structures with high specific surface areas. These materials possess the capability for good physisorption to aromatic and backbone phosphodiester groups, which can be taken as the platform for the adsorption of DNA chains.

The monolayer or multilayer MnO_2 nanosheets have especially attractive properties due to the resemblance of their structures to graphene.[71] The adsorption effect of MnO_2 nanosheets on single-stranded DNA (ssDNA) is greater than that on double-stranded DNA (dsDNA). In the absence of the target, the MnO_2 nanosheets adsorb the fluorophore-labeled ssDNA and quench the fluorescence of the fluorophore; in the presence of the target, the configuration of the fluorophore-labeled ssDNA changes to dsDNA, which are released from the MnO_2 nanosheets and the fluorescence of the fluorophore is restored. Yuan *et al.*[72] utilized the MnO_2 nanosheet as a label-free nanoplatform for homogeneous biosensing. Two biosensors based on MnO_2 nanosheets with favorable performances were constructed for ochratoxin A (OTA) and cathepsin D (Cat D) using different probes and following different sensing principles (Fig. 6A). The sensors constructed on this nanoplatform can be applied in not only aqueous solutions but also complicated sample matrixes with favorable sensing performances, high robustness and easy operations. In addition, the MnO_2 nanoplatforms can easily be adapted to other luminescent materials and diverse probes, and therefore wide applications in bio-/chemo-sensing can be expected. Due to the interaction between the bases in nucleic acids and metal ions, the MnO_2 nanosheet as a label-free nanoplatforms can successfully detect Ag^{+}[73] and Hg^{2+}.[74,75] For example, the Zhang *et al.*,[73] for the first time, have developed a MnO_2 nanosheet-assisted ligand–DNA interaction-based fluorescence polarization method for the sensitive detection of Ag^{+} (Fig. 6B). The good linearity ranges from 30–240 nM for Ag^{+} were observed with a detection limit (S/N = 3) of 9.1 nM. This method additionally exhibits high selectivity. This present study has opened up an avenue for determining other analytes, combining the advantages of MnO_2 and the detection of strategy-fluorescence polarization.

In recent years, with the rapid development of various new technologies such as amplification or coupling technique,

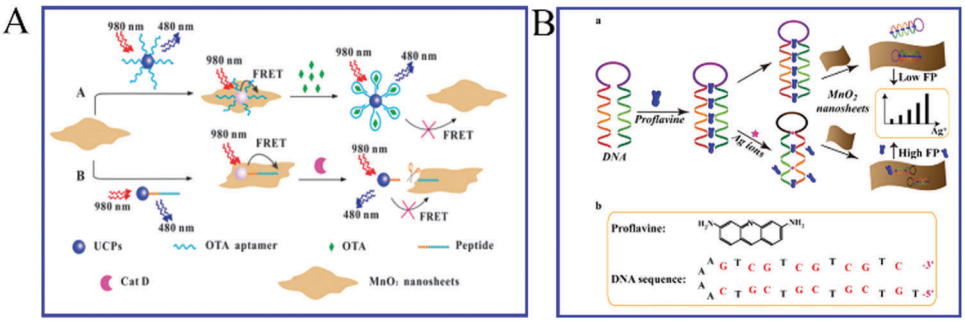

Fig. 6 (A) Schematic illustration (not to scale) of MnO_2 nanosheets-based FRET sensing: the OTA sensor with an ssDNA as the probe and the Cat D sensor with a peptide as the probe. Reproduced from ref. 72 with permission from Royal Society of Chemistry. (B) Illustration of MnO_2 nanosheet-assisted ligand–DNA interaction-based fluorescence polarization sensor for the detection of Ag^{+} ions. Adapted with permission from ref. 73. Copyright (2017) Elsevier.

the combination of nanometer-sized MnO_2 materials with these novel techniques can overcome the drawbacks of conventional sensors and further improve the sensitivity and selectivity of the sensor, which can serve as an effective sensing platform for the detection of small molecules or intracellular substances, and broaden the application of nanometer-sized MnO_2. Xiang *et al.*[76] have developed an in-cell signal amplification approach for monitoring down-regulated miRNAs in living cells based on the biodegradable MnO_2 nanosheet-mediated and target-triggered assembly of hairpins. MnO_2 nanosheets are graphene-like structure nanomaterials that adsorb and exhibit efficient fluorescence quenching ability toward organic dye-linked ssDNAs. The degradation of the MnO_2 nanosheets by intracellular GSH and displacement reactions by proteins or nucleic acids lead to the release of the free hairpins from HCR, resulting in significantly amplified FRET signals from trace miRNA-21 in living cells. The developed method based on the MnO_2 nanosheet-mediated amplification strategy can offer new opportunities for monitoring various trace intracellular miRNA targets in living cells. This MnO_2 sensing platform can be developed for various targets such as DNA,[16,77] RNA,[78] biomolecules[15] and metal ions.[74] The high selectivity can be achieved by quenching the fluorescence of MnO_2 nanosheets and recovering the fluorescence upon adding the targets.

MnO_2 nanosheet-based colorimetric biosensors

The colorimetric biosensor has attracted considerable interest in biological science and analytical chemistry because of the potential for unaided visual readout. There are many advantages such as simplicity, cost-effectiveness and no requirement for any sophisticated instruments, so it is especially meaningful for on-site detection in real time.[79] Among various colorimetric systems, because of its label-free nature and fast response, the enzyme catalytic oxidation of a chromogenic substrate such as 3,3′,5,5′-tetramethylbenzidine (TMB) has been widely applied in colorimetric biosensing. In recent years, artificial enzymes have been of great interest due to their enzyme-like reaction profiles and substrate specificities, which are more robust, stable, and tunable as compared with natural enzymes.

MnO_2 nanomaterials have high peroxidase-, oxidase-, and catalase-like activities due to the presence of lattice oxygen defects that were recently found to be capable of catalyzing the reaction of organic substrates [(TMB), *o*-phenylenediamine (OPD), and diazoaminobenzene (DAB)] in the absence of H_2O_2 to produce a color reaction.[80] Based on this oxidase-like catalytic property, different groups have reported that MnO_2 nanomaterial exhibited oxidase-like activity for the colorimetric detection of various analytes, including ions, small molecules, *etc.*

Liu *et al.*[23] reported that MnO_2 nanosheets possess oxidase-like activity that can catalyze the oxidization of TMB. Meanwhile, the existence of GSH can cause the reduction of oxidized TMB, which will generate a visual color change (Fig. 7A). Thus, the authors developed a novel colorimetric method for detecting GSH with a limit of detection of 300 nM in human serum. Its convenience and visibility will be very important for biomedical applications. Similarly, the MnO_2 nanosheet–TMB reaction system was developed as a convenient detection platform for other antioxidants like uric acid,[81] ascorbic acid,[82] cysteine, *etc.* Nevertheless, these sensors only determine a single antioxidant, which does not allow high-throughput detection owing to their similar chemical properties.

Array-based sensing approaches using nanomaterials have emerged as a powerful tool for the discrimination of a variety of analytes with similar structures and properties. Combining the advantages of the array-based sensing and MnO_2 nanosheet–TMB reaction system, He *et al.*[18] reported a unique visual

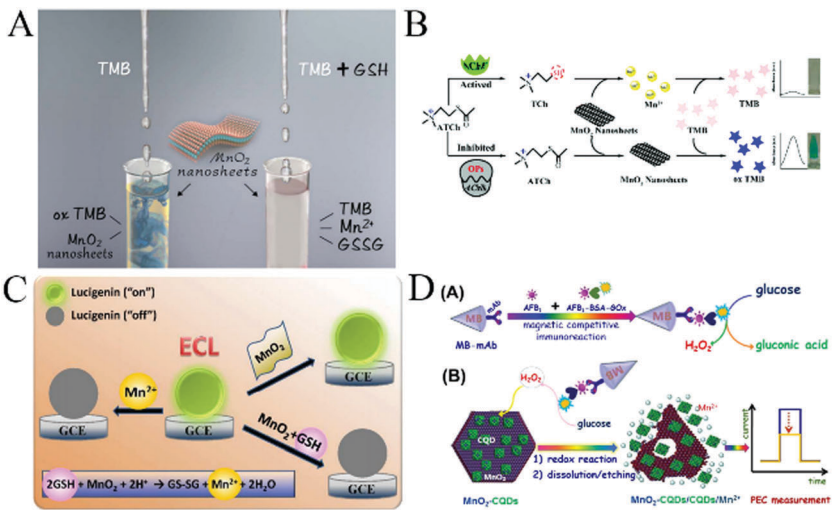

Fig. 7 (A) Illustration of the MnO_2 nanosheet-based colorimetric assay for GSH quantification. Adapted with permission from ref. 23. Copyright (2017) Elsevier. (B) Schematic of a colorimetric platform for AChE activity and its inhibitor. Reproduced ref. 84 with permission from Royal Society of Chemistry. (C) Schematic illustration for measuring GSH using lucigenin and MnO_2 nanosheets. Adapted with permission from ref. 22. Copyright (2016) American Chemical Society. (D) Schematic illustration of the photoelectrochemical immunosensing platform toward aflatoxin B1 (AFB1) on carbon quantum dots-coated MnO_2 nanosheets (MnO_2–CQDs) by coupling an enzyme immunoassay format with a magneto-controlled microfluidic device. Adapted with permission from ref. 96. Copyright (2017) American Chemical Society.

colorimetric sensor array for the discrimination and identification of five antioxidants with the help of statistical analysis in serum. In this study, they employed MnO_2 nanosheets to trigger a multicolor chromogenic system for discriminating five antioxidants. Different antioxidants have distinct reducing abilities, producing different inhibitions on the MnO_2 nanosheet–TMB system, and therefore generating distinct colorimetric response patterns at 370, 450, and 650 nm. Using this sensor array, five antioxidants including UA, GSH, AA, Cys and Mel were successfully discriminated at a low concentration of 20 μM. Meanwhile, fetal bovine serum spiked with different antioxidants can be directly differentiated with the naked eye. Furthermore, this sensor array can also discriminate different concentrations of antioxidants and antioxidant mixtures and may hold great promise for the medical diagnosis and antioxidant biosensor.

Based on the strong affinity between thiolated compounds and metal ions, several studies have developed methods for metal ion detection in aqueous solution. Ye *et al.*[83] prepared homogeneous MnO_2 nanorods as oxidase-like mimetics to catalyze the oxidation of TMB into a blue colored cation radical in the absence of H_2O_2. GSH can successfully hinder the cation radical production leading to the decrease of solution absorbance, and mercury ions (Hg^{2+}) have a strong affinity for thiolated compounds, therefore, when GSH and Hg^{2+} were pre-incubated, the solution was recovered to the blue colored solution in the presence of MnO_2 nanorods. Based on this, the authors developed a simple and novel "off–on" colorimetric sensor for the detection of Hg^{2+} in aqueous solution and real water samples with a good linear relationship from 0.1 to 8.0 μM. The limit of detection was estimated to be 0.08 μM. The catalytic reaction was fast and the visible color change of the reaction system is obvious. The proposed method opens up a new possibility for monitoring trace levels of metal ions in real samples.

Although a large number of documents have reported the detection of different substances in chem/biosensing applications based on the MnO_2–TMB strategy as a promising platform, there are few reports about the detection strategy that combines the specificity of the enzyme with the MnO_2-catalyzed visual detection. Yan[84] designed a novel colorimetric sensing platform using the specific reaction between thiocholine and the MnO_2–TMB platform for the quantitative detection of acetylcholinesterase (AChE) activity and its inhibitor (Fig. 7B). First, the probe was constructed using MnO_2 nanosheets as an oxidase-mimicking nanomaterial to directly oxidize TMB to oxTMB. In the presence of AChE, acetylthiocholine (ATCh) was catalytically hydrolysed to thiocholine (TCh), which easily triggered the decomposition of MnO_2 nanosheets, and rendered TMB molecules colourless. When organophosphorus pesticides (OPs) were introduced, the activity of the enzyme was suppressed, preventing the generation of TCh and the decomposition of MnO_2, resulting in the increase in the absorbance. By monitoring the absorbance change, they can quantitatively detect AChE activity and its inhibitor paraoxon. The integration of these two strategies not only enhanced the selectivity and sensitivity of the colorimetric sensing probe but also provided a novel strategy for enzyme detection. More importantly, the MnO_2–TMB platform can also be successfully utilized in fabricating test strips for on-site monitoring of AChE activity and its inhibitor with high sensitivity and good accuracy, which also provides a new way to detect AChE activity and other organophosphorus pesticides.[85]

MnO_2 nanosheet-based electrochemical biosensors

MnO_2 has been explored as an alternative electrochemical catalyst for fabricating enzyme-free and sensitive electrochemical sensors due to its peculiar properties, including high catalytic activity, good chemical stability, low-cost, environmental friendliness and high energy density. However, the low intrinsic electrical conductivity of MnO_2 (10^{-5}–10^{-6} S cm^{-1}) encourages researchers to combine MnO_2 with graphene oxide,[86] carbon nanotubes (CNTs),[87] carbon foam,[88] metal nanoparticles or metal oxides,[89] *etc.* Thus, by combining the advantages of the remarkable electrical conductivity and excellent biocompatibility of graphene with the high electrocatalytic activity of MnO_2, the synergistic effect between them can make it possible to fabricate a sensor with good performance in the detection of various analytes, including ions, small molecules, immunoassays and so on. Specifically, MnO_2 has a well-known electrochemical activity on H_2O_2 decomposition.

Feng *et al.*[90] developed the petal-shaped MnO_2 nanosheet/graphene composites as an electrode material for the nonenzymatic sensing of H_2O_2 in a neutral environment. The fabricated sensor showed good repeatability, stability, selectivity, and high catalytic activity for the detection of H_2O_2. This assay has excellent anti-interference ability and displayed two wide linear ranges from 10 to 90 μM and from 0.2 to 0.9 mM with a low detection limit of 2 μM. In order to measure the trace concentration of H_2O_2 released by living cells/organisms, there is an urgent need to develop a much more sensitive electrochemical sensor based on a desirable nanomaterial with a unique electrocatalytic activity. Hu *et al.*[91] successfully prepared MnO_2 nanosheets with enhanced specific surface area and porous structure by a facile and efficient method, which is beneficial for their applications as electrochemical sensing materials. The H_2O_2 electrochemical nonenzymatic sensor was constructed based on MnO_2 nanosheets to monitor H_2O_2 released by living cells. The proposed biosensor is highly sensitive and selective for the determination of H_2O_2 with a detection limit of 5 nM. The constructed electrochemical nonenzymatic sensor has been successfully applied to the real-time monitoring of the trace concentrations of H_2O_2 (0.1 μM) released by SP2/0 cells. The present study has shown that MnO_2 nanosheets provide a new platform for developing highly sensitive electrochemical sensors with practical applications.

A recent striking find by Duan[92] is that amorphous MnO_2 can be used as a highly effective water oxidation catalyst to evolve molecular oxygen, which can quench the ECL for deactivating the excited state of $Ru(dcbpy)_3^{2+}$. Based on the properties, Yuan *et al.*[86] first described a signal-on electrochemiluminescence (ECL) aptasensor for the ultrasensitive detection of carcinoembryonic antigen (CEA) by using surface-initiated atom transfer

radical polymerization (SI-ATRP) to facilitate the high density immobilization of a luminophore ($Ru(dcbpy)_3^{2+}$-pendant PAMAM–poly-GMA) and manganese dioxide–graphene (MnO_2–GO) composite, which can indirectly deactivate the excited state of $Ru(dcbpy)_3^{2+}$. Due to the synergistic contribution of two functional components, the MnO_2–GO composite can serve as an effective quencher for $Ru(dcbpy)_3^{2+}$. The aptasensor has a good linear response for CEA ranging from 0.1 pg mL^{-1} to 20 ng mL^{-1} with a limit of detection of 25.3 fg mL^{-1}. In addition, the ECL aptasensor exhibited high sensitivity, good stability, and satisfying selectivity, which provided a promising alternative tool for the determination of proteins in clinic analysis.

MnO_2 nanosheets have little effect on the ECL of lucigenin. However, Mn^{2+} can obviously inhibit the ECL of lucigenin. Based on this principle, Gao *et al.*[22] developed a new ECL method for the highly sensitive detection of GSH in human serum samples using lucigenin as the ECL luminophore and MnO_2 nanosheets as the mediator. When MnO_2 nanosheets were reduced to Mn^{2+} by GSH, an obvious inhibition on the ECL of lucigenin was observed. The ECL inhibition efficiencies gradually increased when the concentrations of GSH increased from 10 to 2000 nM. This nanosystem possessed a good linear relationship and the detection limit is 3.7 nM (Fig. 7C). This proposed method is highly sensitive, simple, fast, selective, and cost-effective. Besides, it is reported that this is the first time MnO_2 nanosheets were used in the ECL detection technique, and it will stimulate the development of other ECL detection platforms.

The photoelectrochemical (PEC) sensing method is a newly grown and booming detection technique.[93,94] It combines the advantages of optical methods and electrochemical sensors, and thus shows great promise in analytical applications. Owing to its band gap of about 2.1 eV, MnO_2 nanosheets exhibit unique electrochemical properties and have an absorption peak centered at around 380 nm, which tails into the visible region. Sasaki *et al.*[95] reported the observation of photocurrent generation *via* self-assembled MnO_2 nanosheets on indium tin oxide (ITO) under visible light irradiation in nonaqueous electrolyte. Due to the strong localized d–d transition and high contact resistance, only a poor photocurrent from MnO_2 nanosheets can be observed. Based on this study, Lin *et al.*[96] designed MnO_2–CQDs hybrid nanostructures for the improvement of photoelectrochemical properties (Fig. 7D). In this work, they developed a proof-of-concept high-throughput PEC immunosensing system for the simultaneous quantitative visual detection of AFB1 (as a model mycotoxin) by coupling a semiautomatic microfluidic device with the nanoparticles-based immunoassay format. In the presence of target AFB1, it initially competed with AFB1–BSA–GOx for the labeled anti-AFB1 antibody on the magnetic beads, and then the carried GOx oxidized the glucose to generate H_2O_2. In this case, the produced H_2O_2 was used as the reducing agent for the decomposition of MnO_2 nanosheets. Due to the decline of MnO_2–CQDs on the electrode, the photocurrent of the MnO_2–CQDs-modified electrode decreased with the increasing H_2O_2 concentration. By monitoring the change in photocurrent, we can quantitatively determine AFB1 in real samples. MnO_2–CQDs were favorably eliminated, and a visual detection could be realized by judging the color intensity change of the electrode. Due to the synergism between MnO_2 and CQDs, the PEC activity of MnO_2 and the efficiency of PEC sensors have been greatly improved. This present system has opened up new horizons for determining other mycotoxins or small molecules by changing the corresponding conditions.

MnO_2 nanosheet-based bioimaging

Molecular imaging as a non-invasive tool is the most attractive imaging technique for the early detection and management of malignant tumors. Due to the poor tissue penetration of ''turn-off'' fluorescence imaging and the poor sensitivity of magnetic resonance imaging (MRI), two or more imaging techniques are combined to synergistically address multiple issues like sensitivity, resolution, and tissue penetration in tumor diagnosis. However, these ''always on'' imaging probes still suffer from a high non-specific background and a low signal to background ratio. To address these issues, the use of activatable imaging probes may cater to the improvement of the signal to background ratio, sensitivity, and specificity.[97]

As two-dimensional materials, MnO_2 nanosheets have a large specific surface area and a broad absorption spectrum, which has been widely used as the fluorescence quencher. Moreover, since MnO_2 can achieve controlled degradation in the tumor microenvironment under the condition of low pH and high GSH concentrations, the fluorescence quenched by MnO_2 can be recovered once MnO_2, a high T_1-weighted contrast agent with excellent MRI characteristics, is reduced to Mn^{2+}, enabling the imaging intensity to be controllable. MnO_2 nanomaterials, therefore, have shown great prospects as activatable bioimaging platforms. Recently, several MnO_2 nanostructure-based activatable bioimaging platforms have been reported for intracellular or *in vivo* imaging.

Lee *et al.*[98] developed urchin-shaped MnO_2 nanomaterials as pH-responsive activatable T_1 contrast agents for *in vivo* MRI imaging with a mouse tumor model. Based on that, Chen *et al.*[99] explored the degradation of MnO_2 nanosheets under conditions of low pH in tumor cells and confirmed that their degraded Mn^{2+} had magnetic resonance T_1-weighted imaging properties. When DOX–PEG–MnO_2 enters the cell through endocytosis, low pH-responsive MnO_2 decomposed to Mn^{2+}, which acts as a highly efficient T1-MRI CAs for *in vivo* nude mice tumor imaging. The anticancer drug, DOX, was released into the acidic microenvironment of the tumor tissue, inducing remarkable apoptosis and achieving the successful theranostics of cancer in an intelligent and on-demand manner (Fig. 8A). T1-MRI images were observed at the axial and coronal sites of 4T1 tumor-bearing nude mice before and after administration of PEG–MnO_2 nanosheets within the tumor and normal subcutaneous tissue every 10 min. Quantitative T1-MRI signal intensity was recorded before and after the administration of PEG–MnO_2 nanosheets on the (c) axial tumor region and (d) coronal tumor region and normal subcutaneous tissue. In order to make up for the insufficiency of single MIR imaging, Zhao *et al.*[100] firstly developed a novel dual-activatable fluorescence/MRI bimodal

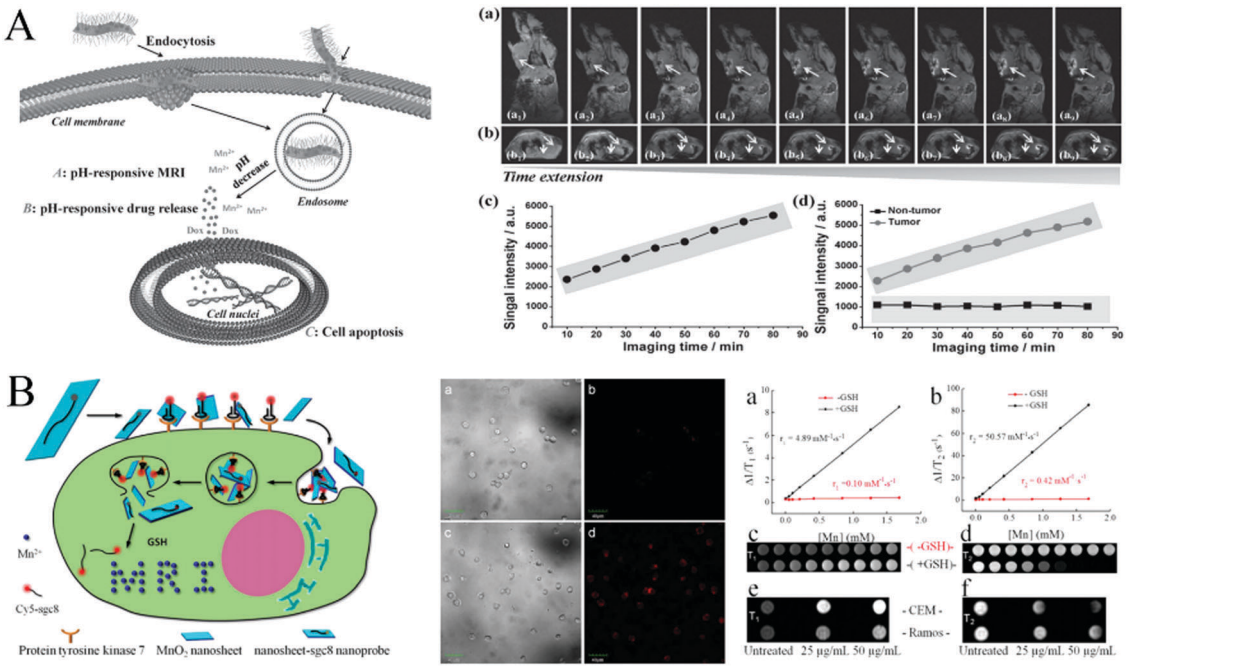

Fig. 8 (A) Theranostic function of PEG–MnO_2 nanosheets for intracellular pH-responsive drug delivery and T1-MRI, and the axial and coronal T1-MRI of 4T1 tumor-bearing nude mice before and after the administration of PEG–MnO_2 nanosheets. Reprinted with permission from ref. 99. Copyright (2014) Wiley-VCH. (B) Activation mechanism of the MnO_2 nanosheet–aptamer nanoprobe for fluorescence/MRI bimodal tumor cell imaging, and the confocal imaging and MRI images of CCRF-CEM cells. Adapted with permission from ref. 100. Copyright (2014) American Chemical Society.

platform for imaging cancer cells using a MnO_2–Cy5-labeled aptamer nanoprobe that can target, recognize and enter tumor cells (Fig. 8B). The overexpressed GSH in tumor cells induced the degradation of MnO_2 and released Cy5-labeled aptamers as well as Mn^{2+}. On the one hand, the released Cy5-labeled aptamers can be used for fluorescence imaging; on the other hand, the produced Mn^{2+} is used as a contrast agent for MRI to increase the contrast signal, which can be used as a dual-activatable fluorescence/MRI bimodal platform in cancer cell imaging. It is demonstrated that the fluorescence activation of the nanoprobe possesses high specificity to target cells by using confocal laser scanning microscopy. The feasibility of a nanosheet–sgc8 nanoprobe for cellular MRI was also evaluated by examination of CCRF-CEM cells (human T cell acute lymphoblastic leukemia cell line cells) and Ramos cells incubated with nanoprobes at different concentrations.

Overall, various imaging modalities and image-enhancing methods based on MnO_2 nanosheets have been developed to provide help in the sensitive detection of cancer in its earliest stages and further their applications in cancer management.

MnO_2 nanosheet-based drug delivery and cancer therapy

MnO_2 nanosheets, as outstanding structural nanomaterials with low toxicity, strong adsorption, large surface-to-volume ratio and good biocompatibility, can load numerous guest molecules. Moreover, MnO_2 nanosheets are degraded by over-expressed GSH at low pH in cancer cells and have been widely used for drug delivery and cancer therapy. Here, we discuss the progress in cancer therapy combining MnO_2 nanostructure-based drug delivery with different methods, including chemotherapy, photodynamic therapy, photothermal therapy and gene therapy.

In recent decades, the drug delivery system (DDS) based on nanomaterials has been widely studied, which provides hope by enhancing the selectivity of chemotherapy. Chemotherapy usually refers to the use of medicines or drugs to treat cancers. Zhao *et al.*[101] designed a novel and facile multifunctional nanocomposite probe (MSU/MnO_2) as a new DDS (Fig. 9A). They first prepared the magnetic up-conversion (MSU) composite probe through conjugated cross-linking of amino-modified Fe_3O_4@SiO_2 particles (the core) and carboxyl functionalized NaYF4: Yb,Er nanoparticles (the shell). Layered MnO_2 nanosheets were formed *in situ* on the surface of MSU as MSU/MnO_2 for the loading and release of the model drug, congo red (CR). In this DDS, the targeted transport of Fe_3O_4 to tumor cells and decomposition of MnO_2 nanosheets in the tumor cells can achieve the release of drugs at the lesion sites. Moreover, the quenched fluorescence was recovered and upconversion luminescence was observed. Similarly, Wang *et al.*[20] have used the redox-responsive degradable MnO_2 nanostructures as an effective nanocarrier for detecting intracellular glutathione and triggering doxorubicin (DOX) release.

Chemotherapy may have serious side effects on normal cells and tissues due to the lack of selectivity, which can limit their applications in cancer treatment. Better DDS should have the characteristic of the controllable release at a target position. By conjugating the targeting ligand of the tumor-specific receptors on the surface of nanoparticles, active tumor targeting has successfully improved the tumor targeting efficiency. In recent years, some natural target molecules such as folic acid (FA) and

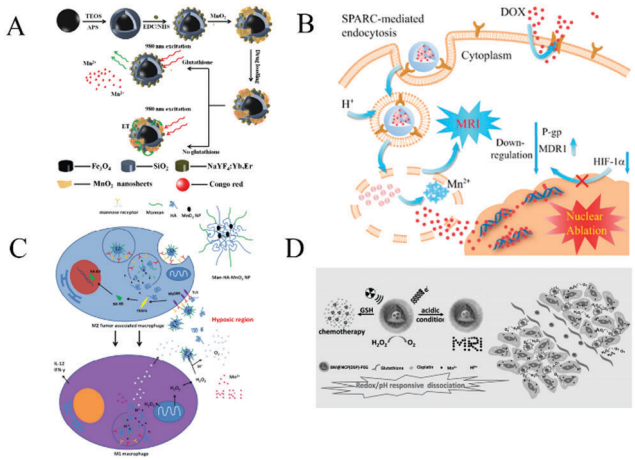

Fig. 9 (A) Schematic illustration of the synthetic procedure for the preparation of the MSU/MnO_2-CR drug delivery system. Reproduced from ref. 101 with permission from the Royal Society of Chemistry. (B) Schematic illustration of BMDN as an MDR-reversal vector and T_1-weighted contrast agent for MRI and simultaneous chemotherapy on the resistant tumor. Adapted with permission from ref. 102. Copyright (2017) American Chemical Society. (C) Bioconjugated manganese dioxide nanoparticles enhanced the chemotherapy response by priming tumor-associated macrophages toward the M1-Like phenotype and attenuating tumor hypoxia. Adapted with permission from ref. 103. Copyright (2016) American Chemical Society. (D) A scheme illustrating the redox/pH-responsive behaviors of BM@NCP(DSP)–PEG composite nanoparticles in the tumor microenvironment. Reprinted with permission from ref. 104. Copyright (2017) Wiley-VCH.

hyaluronic acid (HA) have made great progress in the research on tumor targeting. They are widely applied in the extracellular matrix, cell surface and intracellular matrix of various body tissues, and can specifically bind to receptors that are highly expressed on the surface of tumor cells. In this way, targeted cancer therapy can be achieved without any complex nanomaterials.

Zhang *et al.*[25] developed a multifunctional tumor targeting theranostic system for tumor-targeting therapy and magnetic resonance imaging by employing FA as an attractive targeting agent. Layered MnO_2 nanosheets have been used as drug nanocarriers and potential magnetic resonance imaging (MRI) agents. The MnO_2–PEG–FA/DOX nanosheets are highly efficient for delivering doxorubicin (DOX) to tumor cells *in vitro* and *in vivo* due to the presence of the folate receptors, meanwhile, MnO_2 can be quickly decomposed into Mn^{2+}, enabling magnetic resonance imaging under the slightly acidic environment with a high concentration of GSH. By taking advantage of active targeting and efficient MRI in multiple reductions, pH dual-responsive biodegradable nanosheet systems have provided a promising platform for tumor-targeting theranostics. Similarly, BSA–MnO_2–DOX nanomaterials (BMDN) were fabricated by Chen *et al.*[102] as the DOX drug loading nanoplatform for cancer magnetic resonance imaging and simultaneously reversing multidrug resistance in the resistant tumor (Fig. 9B). BMDN facilitated the delivery of DOX into MDR tumor cells through their MDR reversal effects including enhanced cellular uptake, reduced drug efflux, and a decreased hypoxic tumor microenvironment. BMDN also acted as an effective MRI contrast agent, thereby causing good *in vitro* and *in vivo* T_1-weighted imaging.

Liu[103] constructed HA-modified mannan-conjugated MnO_2 nanoparticles (Man–HA–MnO_2 NPs) as the target delivery platform to alleviate tumor hypoxia and enhance chemotherapy response by reacting with endogenous H_2O_2 under hypoxic conditions. Combination treatment of the tumors with Man–HA–MnO_2 NPs and doxorubicin significantly increased the apparent diffusion coefficient values for breast tumors, largely inhibited tumor growth and tumor cell proliferation as compared with chemotherapy alone. In addition, the released Mn^{2+} ions have the ability to highly enhance T1 MRI performance for tumor imaging (Fig. 9C). Liu[104,105] *et al.* has utilized the nanoscale-coordination-polymer-shelled MnO_2 composite nanomaterials as a multistage redox/pH/H_2O_2-responsive nanoplatform for cancer chemoradiation treatment (Fig. 9D). The MnO_2-based multifunctional drug carrier nanoplatform not only broadens the application of the MnO_2 nanomaterials but also provides a new approach for the simultaneous magnetic resonance imaging and cancer therapy.

Compared with chemotherapy, photodynamic therapy (PDT) is a form of phototherapy that is based primarily on the production of reactive oxygen species by photosensitizing molecules under selective illumination and is, therefore, toxic to target tissues. PDT is a minimally invasive treatment strategy to kill tumors with high specificity. It has received tremendous attention over the past decades in both preclinical studies and clinical practices.[106] Tan *et al.* have developed a series of drug delivery and cancer treatment platforms based on MnO_2 nanocomposites. For example, Meng *et al.*[67] developed a detecting platform for GSH bioimaging in CEM cells and tissues based on activatable two-photon mesoporous silica (TP-MSNs) coated with MnO_2 nanosheets fluorescence nanoprobes. Later, they improved the abovementioned work and obtained multi-functional nanoprobes for contrast-enhanced dual-mode cell imaging and targeted therapy.[19] In the later work, MSNs were loaded with antitumor drug DOX and photosensitizer molecule chlorin e6 (Ce6). The Sgc8 aptamer for targeted cancer cells was adsorbed on the surface of MnO_2 nanosheets. In addition, MnO_2 nanosheets acted not only as a gatekeeper for TP-MSNs, but as a quencher for TP fluorescence and a contrast agent for MRI. Due to the abovementioned effects, this design can be used not only for intracellular GSH imaging but also for targeting CEM cells. It can achieve the release of DOX and Ce6 from MSN in cancer cells, as well as the synergistic effect of chemotherapy and PDT.

Fan *et al.*[107] found that the concentration of intracellular GSH was related to the content of singlet oxygen ($^1O_2$), which was generated through the reaction between a photosensitizer and tissue oxygen under illumination. Based on this fact, they constructed a multifunctional photosensitizer chlorin e6 (Ce6)–MnO_2 nanosystem. It not only inhibits extracellular singlet oxygen generation by Ce6 with fewer side effects but can also enhance the cellular uptake of photosensitizers for highly efficient intracellular PDT as compared to free Ce6. As seen in Fig. 10A, the level of GSH is decreased in cancer cells *in situ*, causing the death of cancer cells. Moreover, flow cytometry and

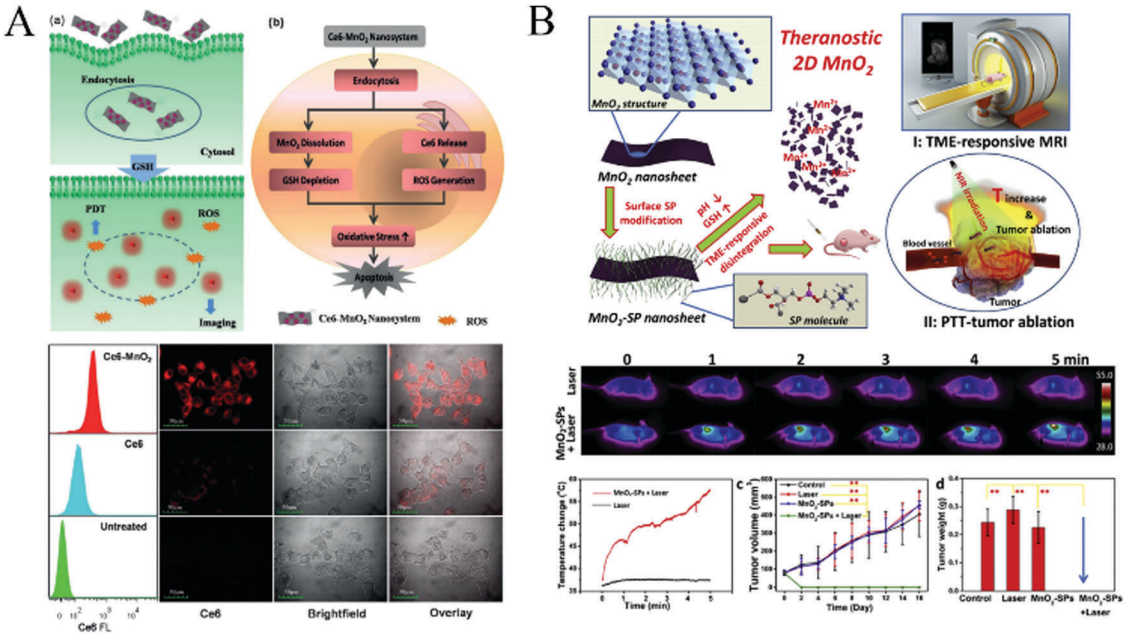

Fig. 10 (A) Activation mechanism of the Ce6–MnO_2 nanosystem for highly efficient photodynamic therapy, and flow cytometry analysis (left) and confocal fluorescence images (right) of MCF-7 cells treated with free Ce6 and the Ce6–MnO_2 nanosystem. Reprinted with permission from ref. 107. Copyright (2016) Wiley-VCH. (B) Schematic illustration of the synthetic procedure for MnO_2-SPs nanosheets and their specific functions for tumor theranostics with TME sensitivity, including the acidic/reducing condition-triggered T_1-weighted MR imaging and efficient PTT against the tumor, and the *in vivo* photothermal therapy against tumor growth assisted by MnO_2-SPs. Adapted with permission from ref. 108. Copyright (2018) Elsevier.

confocal laser scanning microscopy analysis of cells treated with the Ce6–MnO_2 nanosystem both presented significantly higher fluorescence intensity in the cytoplasm as compared to untreated cells and cells treated with only Ce6. These results also demonstrated that the Ce6–MnO_2 nanosystem was mainly distributed in the cytoplasm, and MnO_2 nanosheets were mainly reduced by the GSH in the cytoplasm. The data suggest that the MnO_2 nanosheets can efficiently deliver photosensitizer Ce6 into cells for photodynamic therapy. Moreover, this multifunctional MnO_2 nanosheet nanosystem shows significant promise in monitoring various types of cancers and facilitating their biomedical applications, particularly cancer theranostics.

Coincidentally, photodynamic therapy based on multifunctional MnO_2 nanocarriers was also published by other groups. Liu[27] further conjugated MnO_2 nanomaterial with amino terminated polyethylene glycol (PEG–NH_2) to increase its water solubility and physiological stability. They combined the advantages of the high reactivity of MnO_2 nanomaterials toward endogenous H_2O_2 within the tumor microenvironment to generate O_2 and multifunctional Ce6@MnO_2–PEG to achieve enhanced tumor-specific PDT and MR imaging in the solid tumor microenvironment.

Premature leakage of photosensitizer (PS) from nanocarriers significantly reduces the accumulation of PS within a tumor, thereby increasing the nonspecific accumulation in normal tissues and inevitably leading to a limited efficacy for PDT and the more apparent systemic phototoxicity. Ma *et al.*,[26] for the first time, designed an intelligent core–shell PDT nanoplatform utilizing SiO_2–methylene blue (MB) with a high MB payload as the inner core and MnO_2-based nanostructures as the intelligent "gatekeeper". This method prevents the premature release of loaded PS in the core and elevates the O_2 concentration for the *in vivo* imaging-guided PDT and MRI imaging by stimuli-responsive acidic H_2O_2 in solid tumors. This proof of concept might provide a novel route to develop the new tumor microenvironment-sensitive nanoplatform for imaging-guided cancer therapy.

Although PDT has become an excellent strategy in cancer treatment, it still faces problems such as poor tumor selectivity, hypoxia-induced drug resistance, and limitations of common photosensitizers. Photothermal therapy (PTT) can significantly inhibit the growth of cancer cells by photothermal ablation and also greatly enhance the efficacy of chemotherapy and PDT. In order to overcome the shortcomings of photodynamic therapy and achieve photothermal (PTT) therapy triggered on cancer cells under near-infrared light irradiation, Liu *et al.*[108] reported a new finding that ultrathin 2D MnO_2 nanosheets, as a new photothermal agent, intrinsically possess high photothermal-conversion capability for highly efficient PTT against tumors. Moreover, these ultrathin MnO_2 nanosheets exhibited an ultrasensitive response to the endogenous tumor microenvironment (TME), which can disintegrate and release the Mn^{2+} in response to the low pH and high concentration of GSH for T_1-weighted MR imaging of the tumor. Through the recording of IR thermal images, the tumor surface temperature of the MnO_2-SPs + Laser group increased from 37 °C to 57 °C within 5 min under NIR laser irradiation, while the temperature of the laser-only group just increased by 1 °C.

Digital photos, tumor size and body weight of 4T1 tumor-bearing mice in four groups were recorded every other day for

16 days after different treatments. It was noted that the tumors were completely eliminated after the MnO_2-SPs injection combined with 808 nm laser irradiation without obvious reoccurrence on the 16th-day feeding, which was further demonstrated by the tumor weight at the end of the evaluation (Fig. 10B). The high PTT efficiency of 2D MnO_2 nanosheets responding to exogenous NIR irradiation has been systematically demonstrated both *in vitro* and *in vivo* to suppress the tumor growth.

Gene therapy is becoming a promising approach for the treatment of both inherited and acquired diseases. Fan *et al.*[109] employed MnO_2 nanosheets as nanocarriers loaded with DNAzymes for gene silencing therapy and cell imaging (Fig. 11). They applied the photosensitizer Ce6 as a PDT agent, and free Mn^{2+} ions could then be used as efficient cofactors of 10–23 DNAzyme for gene silencing. Based on these, they constructed the photosensitizer Ce6–MnO_2–DNAzymes nanosystem for highly efficient photodynamic therapy (PDT) and gene silencing therapy by consuming intracellular GSH and protecting reactive oxygen species, which can be used to kill cancer cells.[26] As shown in confocal laser scanning microscopy analysis (Fig. 11B), comparing the internalization of the Ce6–DNAzyme–MnO_2 nanosystem and that of free DNAzyme in MCF-7 breast-cancer cells, MCF-7 cells treated with the MnO_2 nanosheets can efficiently deliver Ce6-labelled DNAzymes into cells for therapeutic applications. In addition, as shown in Fig. 11C and D, an MTS assay and a soft-agar colony assay were applied to investigate the proliferation of MCF-7 cells treated with a nanosystem containing different concentrations of DNAzymes. It was found that compared with the DNAzyme only, the gene silencing therapeutic efficacy of the DNAzyme–MnO_2 nanosystem gradually increased with increasing concentration of DNAzyme. These results show that the MnO_2 nanosheet is both a potent delivery tool and an efficient cofactor to facilitate DNAzyme-based gene-silencing therapy.

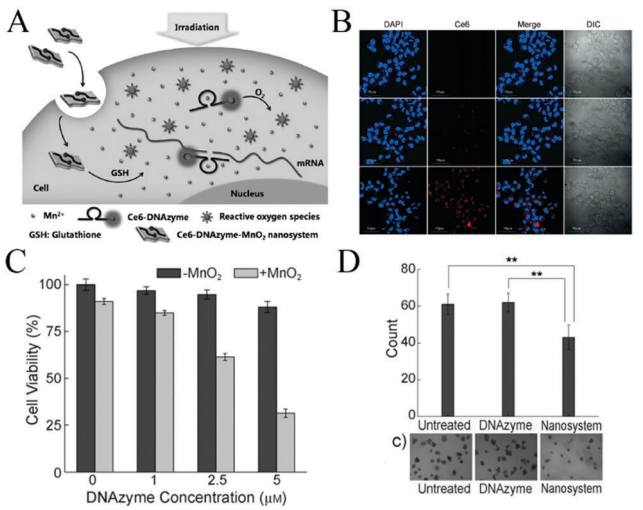

Fig. 11 (A) Activated mechanism of the Ce6–DNAzyme–MnO_2 nanosystem for gene silencing and PDT. The nanosheet can adsorb and efficiently deliver DNAzymes into cells and protect them from enzymatic digestion. (B) Confocal fluorescence images of MCF-7 cells without treatment (upper) and with treatment with Ce6–DNAzyme (middle) and the Ce6–DNAzyme–MnO_2 nanosystem (lower). (C) Gene-silencing therapy with the DNAzyme–MnO_2 nanosystem. (D) Statistical analysis of results from the soft-agar colony assay. (A–D) Reprinted with permission from ref. 109. Copyright (2015) Wiley-VCH.

The properties of the MnO_2 composite material were highly improved, and *in vitro* and *in vivo* detection/imaging indicated their successes as biodegradable probes. These studies have shown the promise of using MnO_2 nanosheets for bioimaging, drug delivery, diagnosis and therapy, and should encourage in-depth studies of MnO_2 composite nanomaterials for other biomedical applications.

Summary and outlook

In this review, we discussed the recent advances of MnO_2 nanosheets-based biochemical application platforms, from the preparation of MnO_2 nanosheets to chemical/biomedical applications including fluorescence biosensors, electrochemical biosensors, colorimetric biosensors, bioimaging, drug delivery and cancer therapy. Although MnO_2 nanomaterials have been widely studied in recent years, compared with GO and other two-dimensional nanomaterials, most of the research on MnO_2 nanosheets is still at the primary stage. The prospects for popularizing their related clinical products is infinite. Several unresolved issues and further research efforts for the future are listed in the following.

(I) In terms of the preparation method, manganese dioxide is mostly prepared by one-pot synthesis, from which pristine MnO_2 nanomaterial is obtained. Some physical or chemical exfoliating methods were adopted to obtain the lamellar MnO_2, whose size, composition and dispersibility have not been determined. More controllable and functional strategies should be developed to obtain the desired structural/compositional MnO_2 nanomaterials.

(II) Regarding diagnostics and therapeutics, MnO_2 nanosheets can act as a nanocarrier without orientation, so it should be able to combine with other substances to achieve the targeted doses and bioimaging accuracy.

(III) Understanding the safety of MnO_2 nanosheets toward living organisms for applications in bioimaging, drug delivery and cancer therapy is imperative. Although the toxicity of MnO_2 is probably low as demonstrated, the potential risks, long-term toxicity, cellular-uptake mechanism and metabolic pathway are still unknown. Sufficient attention should be paid to decrease or diminish its toxicity in living organisms and accelerate the biodegradability on the premise of maintaining therapeutic effects in biological systems.

(IV) Research toward the wider application of MnO_2 for biosensors and biomedicine is still in its infancy, so in-depth studies on MnO_2 nanomaterials are urgently needed for other biomedical applications. MnO_2 nanosheets-based biomedical applications still have room for development and there are infinite research opportunities for researchers to explore.

Conflicts of interest

There are no conflicts to declare.

Acknowledgements

This study was supported in part by the National Natural Science Foundation of China (21205108, 21605038), the Foundation for University Key Teacher by Henan Province (2017GGJS007), and the Key Scientific Research Project in Universities of Henan Province (19A150048).

References

1 T. F. Jaramillo, K. P. Jørgensen, J. Bonde, J. H. Nielsen, S. Horch and I. Chorkendorff, *Science*, 2007, **317**, 100–102.
2 (*a*) W. Wen, Y. Song, X. Yuan, C. Zhu, D. Du, A. Asiri and Y. Lin, *Mater. Today*, 2018, **21**, 164–177; (*b*) C. Zhu, D. Du and Y. Lin, *Biosens. Bioelectron.*, 2017, **89**, 43–55.
3 X. Peng, L. Peng, C. Wu and Y. Xie, *Chem. Soc. Rev.*, 2014, **43**, 3303–3323.
4 Y. Chen, C. Tan, H. Zhang and L. Wang, *Chem. Soc. Rev.*, 2015, **44**, 2681–2701.
5 Y. Omomo, T. Sasaki, L. Wang and M. Watanabe, *J. Am. Chem. Soc.*, 2003, **125**, 3568–3575.
6 K. Kai, Y. Yoshida, H. Kageyama, G. Saito, T. Ishigaki, Y. Furukawa and J. Kawamata, *J. Am. Chem. Soc.*, 2008, **130**, 15938–15943.
7 B. A. Pinaud, Z. Chen, D. N. Abram and T. F. Jaramillo, *J. Phys. Chem. C*, 2011, **115**, 11830–11838.
8 W. Zhai, C. Wang, P. Yu, Y. Wang and L. Mao, *Anal. Chem.*, 2014, **86**, 12206–12213.
9 Y. He, W. Huang, Y. Liang and H. Yu, *Sens. Actuators, B*, 2015, **220**, 927–931.
10 H. Sun, K. Xu, M. Huang, Y. Shang, P. She, S. Yin and Z. Liu, *Appl. Surf. Sci.*, 2015, **357**, 69–73.
11 L. Peng, Q. Zeng, B. Tie, M. Lei, J. Yang, S. Luo and Z. Song, *J. Colloid Interface Sci.*, 2015, **456**, 108–115.
12 D. Fan, C. Shang, W. Gu, E. Wang and S. Dong, *ACS Appl. Mater. Interfaces*, 2017, **9**, 25870–25877.
13 Z. Lin, M. Li, S. Lv, K. Zhang, M. Lu and D. Tang, *J. Mater. Chem. B*, 2017, **5**, 8506–8513.
14 (*a*) Q. Y. Cai, J. Li, J. Ge, L. Zhang, Y. L. Hu, Z. H. Li and L. B. Qu, *Biosens. Bioelectron.*, 2015, **72**, 31–36; (*b*) Y. Hu, L. Zhang, X. Geng, J. Ge, H. Liu and Z. Li, *Anal. Methods*, 2017, **9**, 5653–5658.
15 H.-B. Wang, Y. Li, H.-Y. Bai and Y.-M. Liu, *Sens. Actuators, B*, 2018, **259**, 204–210.
16 D. He, X. He, K. Wang, X. Yang, X. Yang, X. Li and Z. Zou, *Chem. Commun.*, 2014, **50**, 11049–11052.
17 X. L. Zhang, C. Zheng, S. S. Guo, J. Li, H. H. Yang and G. Chen, *Anal. Chem.*, 2014, **86**, 3426–3434.
18 W. Huang, Y. Deng and Y. He, *Biosens. Bioelectron.*, 2017, **91**, 89–94.
19 H. M. Meng, L. Lu, X. H. Zhao, Z. Chen, Z. Zhao, C. Yang, X. B. Zhang and W. Tan, *Anal. Chem.*, 2015, **87**, 4448–4454.
20 D. He, X. He, K. Wang, X. Yang, X. Yang, Z. Zou and X. Li, *Chem. Commun.*, 2015, **51**, 776–779.
21 R. Deng, X. Xie, M. Vendrell, Y. T. Chang and X. Liu, *J. Am. Chem. Soc.*, 2011, **133**, 20168–20171.
22 W. Gao, Z. Liu, L. Qi, J. Lai, S. A. Kitte and G. Xu, *Anal. Chem.*, 2016, **88**, 7654–7659.
23 J. Liu, L. Meng, Z. Fei, P. J. Dyson, X. Jing and X. Liu, *Biosens. Bioelectron.*, 2017, **90**, 69–74.
24 Y. He, B. Jiang, J. Chen, Y. Jiang and Y. X. Zhang, *J. Colloid Interface Sci.*, 2018, **510**, 207–220.
25 Y. Hao, L. Wang, B. Zhang, H. Zhao, M. Niu, Y. Hu, C. Zheng, H. Zhang, J. Chang, Z. Zhang and Y. Zhang, *Nanotechnology*, 2016, **27**, 025101.
26 Z. Ma, X. Jia, J. Bai, Y. Ruan, C. Wang, J. Li, M. Zhang and X. Jiang, *Adv. Funct. Mater.*, 2017, **27**, 1604258.
27 W. Zhu, Z. Dong, T. Fu, J. Liu, Q. Chen, Y. Li, R. Zhu, L. Xu and Z. Liu, *Adv. Funct. Mater.*, 2016, **26**, 5490–5498.
28 Y. B. Hahn, R. Ahmad and N. Tripathy, *Chem. Commun.*, 2012, **48**, 10369–10385.
29 L. Wang, Y. Omomo, N. Sakai, K. Fukuda, I. Nakai, Y. Ebina, K. Takada, M. Watanabe and T. Sasaki, *Chem. Mater.*, 2003, **15**, 2873–2878.
30 Y. Oaki and H. Imai, *Angew. Chem.*, 2007, **119**, 5039–5043.
31 X. Feng, Y. Zhang, J. Song, N. Chen, J. Zhou, Z. Huang, Y. Ma, L. Zhang and L. Wang, *Electroanalysis*, 2015, **27**, 353–359.
32 X. Zhang, R. Kong, Q. Tan, F. Qu and F. Qu, *Talanta*, 2017, **169**, 1–7.
33 L. Zhang, J. Lian, L. Wu, Z. Duan, J. Jiang and L. Zhao, *Langmuir*, 2014, **30**, 7006–7013.
34 J.-L. Chen, L. Li, S. Wang, X.-Y. Sun, L. Xiao, J.-S. Ren, B. Di and N. Gu, *J. Mater. Chem. B*, 2017, **5**, 5336–5344.
35 L. Han, P. Liu, H. Zhang, F. Li and A. Liu, *Chem. Commun.*, 2017, **53**, 5216–5219.
36 Z. Liu, K. Xu, H. Sun and S. Yin, *Small*, 2015, **11**, 2182–2191.
37 H. Chen, J. He, C. Zhang and H. He, *J. Phys. Chem. C*, 2007, **111**, 18033–18038.
38 P. Liu, L. Han, F. Wang, X. Li, V. A. Petrenko and A. Liu, *Nanoscale*, 2018, **10**, 2825–2833.
39 X. Liu, Q. Wang, H. Zhao, L. Zhang, Y. Su and Y. Lv, *Analyst*, 2012, **137**, 4552–4558.
40 J. Xie, Y. Zheng and J. Y. Ying, *J. Am. Chem. Soc.*, 2009, **131**, 888–889.
41 X. Peng, Y. Guo, Q. Yin, J. Wu, J. Zhao, C. Wang, S. Tao, W. Chu, C. Wu and Y. Xie, *J. Am. Chem. Soc.*, 2017, **139**, 5242–5248.
42 X. J. Kong, S. Wu, T. T. Chen, R. Q. Yu and X. Chu, *Nanoscale*, 2016, **8**, 15604–15610.
43 (*a*) H.-B. Wang, Y. Chen, N. Li and Y.-M. Liu, *Microchim. Acta*, 2016, **184**, 515–523; (*b*) Z. M. Huang, J. Yang, L. Zhang, X. Geng, J. Ge, Y. L. Hu and Z. H. Li, *Anal. Methods*, 2017, **9**, 4275–4281.
44 F. Zhou, T. Zheng, E. S. Abdel-Halim, L. Jiang and J.-J. Zhu, *J. Mater. Chem. B*, 2016, **4**, 2887–2894.
45 G. Zhao, J. Li, L. Jiang, H. Dong, X. Wang and W. Hu, *Chem. Sci.*, 2012, **3**, 433–437.
46 J. Liu, Y. Chen, W. Wang, J. Feng, M. Liang, S. Ma and X. Chen, *J. Agric. Food Chem.*, 2015, **64**, 371–380.
47 J. Gallo, N. Vasimalai, M. T. Fernandez-Arguelles and M. Banobre-Lopez, *Dalton Trans.*, 2016, **45**, 17672–17680.

48 Y. Xu, X. Chen, R. Chai, C. Xing, H. Li and X. B. Yin, *Nanoscale*, 2016, **8**, 13414–13421.
49 F. Qu, H. Pei, R. Kong, S. Zhu and L. Xia, *Talanta*, 2017, **165**, 136–142.
50 X. Yan, Y. Song, C. Zhu, H. Li, D. Du, X. Su and Y. Lin, *Anal. Chem.*, 2018, **90**, 2618–2624.
51 L. Han, S. G. Liu, X. F. Zhang, B. X. Tao, N. B. Li and H. Q. Luo, *Sens. Actuators, B*, 2018, **258**, 25–31.
52 D. Garg, A. Mehta, A. Mishra and S. Basu, *Spectrochim. Acta, Part A*, 2018, **192**, 411–419.
53 D. He, X. Yang, X. He, K. Wang, X. Yang, X. He and Z. Zou, *Chem. Commun.*, 2015, **51**, 14764–14767.
54 Y. Wang, K. Jiang, J. Zhu, L. Zhang and H. Lin, *Chem. Commun.*, 2015, **51**, 12748–12751.
55 G. Li, N. Lv, J. Zhang and J. Ni, *RSC Adv.*, 2017, **7**, 16423–16427.
56 X. Yan, Y. Song, C. Zhu, J. Song, D. Du, X. Su and Y. Lin, *ACS Appl. Mater. Interfaces*, 2016, **8**, 21990–21996.
57 J. Deng, D. Lu, X. Zhang, G. Shi and T. Zhou, *Environ. Pollut.*, 2017, **224**, 436–444.
58 J. Chen, Z. Huang, H. Meng, L. Zhang, D. Ji, J. Liu, F. Yu, L. Qu and Z. Li, *Sens. Actuators, B*, 2018, **260**, 770–777.
59 Z. Liu, X. Cai, X. Lin, Y. Zheng, Y. Wu, P. Chen, S. Weng, L. Lin and X. Lin, *Anal. Methods*, 2016, **8**, 2366–2374.
60 D. Fan, C. Shang, W. Gu, E. Wang and S. Dong, *ACS Appl. Mater. Interfaces*, 2017, **9**, 25870–25877.
61 Z. Z. Dong, L. Lu, C. N. Ko, C. Yang, S. Li, M. Y. Lee, C. H. Leung and D. L. Ma, *Nanoscale*, 2017, **9**, 4677–4682.
62 X. He, X. Yang, L. Hai, D. He, X. He, K. Wang and X. Yang, *RSC Adv.*, 2016, **6**, 79204–79208.
63 Y. Zhang, C. Zhang, J. Chen, Y. Li, M. Yang, H. Zhou, S. A. Shahzad, H. Qi, C. Yu and S. Jiang, *J. Mater. Chem. B*, 2017, **5**, 4691–4694.
64 J. Sheng, X. Jiang, L. Wang, M. Yang and Y. N. Liu, *Anal. Chem.*, 2018, **90**, 2926–2932.
65 S. Lin, H. Cheng, Q. Ouyang and H. Wei, *Anal. Methods*, 2016, **8**, 3935–3940.
66 T. Xiao, J. Sun, J. Zhao, S. Wang, G. Liu and X. Yang, *ACS Appl. Mater. Interfaces*, 2018, **10**, 6560–6569.
67 H. M. Meng, Z. Jin, Y. Lv, C. Yang, X. B. Zhang, W. Tan and R. Q. Yu, *Anal. Chem.*, 2014, **86**, 12321–12326.
68 N. Li, W. Diao, Y. Han, W. Pan, T. Zhang and B. Tang, *Chem. – Eur. J.*, 2014, **20**, 16488–16491.
69 X. Wang, D. Wang, Y. Guo, C. Yang, X. Liu, A. Iqbal, W. Liu, W. Qin, D. Yan and H. Guo, *Biosens. Bioelectron.*, 2016, **77**, 299–305.
70 K. Radhakrishnan, P. Panneerselvam and A. Ravikumar, *RSC Adv.*, 2017, **7**, 45824–45833.
71 Y. Yuan, R. Li and Z. Liu, *Anal. Chem.*, 2014, **86**, 3610–3615.
72 Y. Yuan, S. Wu, F. Shu and Z. Liu, *Chem. Commun.*, 2014, **50**, 1095–1097.
73 L. Qi, Z. Yan, Y. Huo, X. M. Hai and Z. Q. Zhang, *Biosens. Bioelectron.*, 2017, **87**, 566–571.
74 K. Yang, M. Zeng, X. Hu, B. Guo and J. Zhou, *Analyst*, 2014, **139**, 4445–4448.
75 J. Li, B. Du, Y. Li, Y. Wang, D. Wu and Q. Wei, *New J. Chem.*, 2018, **42**, 1228–1234.
76 J. Li, D. Li, R. Yuan and Y. Xiang, *ACS Appl. Mater. Interfaces*, 2017, **9**, 5717–5724.
77 Q. Chen, L. Zhang, F. Jiang, B. Wang, T. Lv, Z. Zeng, W. Wu and S. Sun, *Sens. Actuators, B*, 2017, **244**, 1138–1144.
78 M. Ou, J. Huang, X. Yang, K. Quan, Y. Yang, N. Xie and K. Wang, *Chem. Sci.*, 2017, **8**, 668–673.
79 T. Jiang, Y. Song, D. Du, X. Liu and Y. Lin, *ACS Sens.*, 2016, **1**, 717–724.
80 Z.-M. Huang, Q.-Y. Cai, D.-C. Ding, J. Ge, Y.-L. Hu, J. Yang, L. Zhang and Z.-H. Li, *Sens. Actuators, B*, 2017, **242**, 355–361.
81 J. Pal and T. Pal, *RSC Adv.*, 2016, **6**, 83738–83747.
82 L. He, F. Wang, Y. Chen and Y. Liu, *Luminescence*, 2018, **33**, 145–152.
83 H. Yang, Y. Xiong, P. Zhang, L. Su and F. Ye, *Anal. Methods*, 2015, **7**, 4596–4601.
84 X. Yan, Y. Song, X. Wu, C. Zhu, X. Su, D. Du and Y. Lin, *Nanoscale*, 2017, **9**, 2317–2323.
85 H. Ouyang, Q. Lu, W. Wang, Y. Song, X. Tu, C. Zhu, J. N. Smith, D. Du, Z. Fu and Y. Lin, *Anal. Chem.*, 2018, **90**, 5147–5152.
86 Y. He, Y. Chai, H. Wang, L. Bai and R. Yuan, *RSC Adv.*, 2014, **4**, 56756–56761.
87 H. Begum, M. S. Ahmed and S. Jeon, *RSC Adv.*, 2016, **6**, 50572–50580.
88 S. He, B. Zhang, M. Liu and W. Chen, *RSC Adv.*, 2014, **4**, 49315–49323.
89 W. Xu, S. Xue, H. Yi, P. Jing, Y. Chai and R. Yuan, *Chem. Commun.*, 2015, **51**, 1472–1474.
90 X. Feng, Y. Zhang, J. Song, N. Chen, J. Zhou, Z. Huang, Y. Ma, L. Zhang and L. Wang, *Electroanalysis*, 2015, **27**, 353–359.
91 Y. Shu, J. Xu, J. Chen, Q. Xu, X. Xiao, D. Jin, H. Pang and X. Hu, *Sens. Actuators, B*, 2017, **252**, 72–78.
92 L. Duan, L. Tong, Y. Xu and L. Sun, *Energy Environ. Sci.*, 2011, **4**, 3296–3313.
93 H. Yang, Q. Ming, Z. Tao, M. Ji, L. Shaohua, Z. Xiaodong, Y. Chris and F. Xinliang, *Adv. Mater.*, 2017, **29**, 1604480.
94 E. Gil-Santos, C. Baker, A. Lemaitre, C. Gomez, G. Leo and I. Favero, *Nat. Commun.*, 2017, **8**, 14267.
95 N. Sakai, Y. Ebina, K. Takada and T. Sasaki, *J. Phys. Chem. B*, 2005, **109**, 9651–9655.
96 Y. Lin, Q. Zhou, D. Tang, R. Niessner and D. Knopp, *Anal. Chem.*, 2017, **89**, 5637–5645.
97 J. Li, F. Cheng, H. Huang, L. Li and J.-J. Zhu, *Chem. Soc. Rev.*, 2015, **44**, 7855–7880.
98 K. Taekhoon, C. Eun-Jin, C. Youngjoo, K. Minsik, O. Aram, J. Juhong, L. Eun-Sook, B. Hionsuck, H. Seungjoo, S. Jin-Suck, H. Yong-Min and L. Kwangyeol, *Angew. Chem.*, 2011, **123**, 10777–10781.
99 Y. Chen, D. Ye, M. Wu, H. Chen, L. Zhang, J. Shi and L. Wang, *Adv. Mater.*, 2014, **26**, 7019–7026.

100 Z. Zhao, H. Fan, G. Zhou, H. Bai, H. Liang, R. Wang, X. Zhang and W. Tan, *J. Am. Chem. Soc.*, 2014, **136**, 11220–11223.
101 P. Zhao, Y. Zhu, X. Yang, J. Shen, X. Jiang, J. Zong and C. Li, *Dalton Trans.*, 2014, **43**, 451–457.
102 M. Zhang, L. Xing, H. Ke, Y. J. He, P. F. Cui, Y. Zhu, G. Jiang, J. B. Qiao, N. Lu, H. Chen and H. L. Jiang, *ACS Appl. Mater. Interfaces*, 2017, **9**, 11337–11344.
103 M. Song, T. Liu, C. Shi, X. Zhang and X. Chen, *ACS Nano*, 2016, **10**, 633–647.
104 J. Liu, Q. Chen, W. Zhu, X. Yi, Y. Yang, Z. L. Dong and Z. Liu, *Adv. Funct. Mater.*, 2017, **27**, 1605926.
105 Q. Chen, L. Feng, J. Liu, W. Zhu, Z. Dong, Y. Wu and Z. Liu, *Adv. Mater.*, 2016, **28**, 7129–7136.
106 G. Yang, L. Xu, J. Xu, R. Zhang, G. Song, Y. Chao, L. Feng, F. Han, Z. Dong, B. Li and Z. Liu, *Nano Lett.*, 2018, **18**, 2475–2484.
107 H. Fan, G. Yan, Z. Zhao, X. Hu, W. Zhang, H. Liu, X. Fu, T. Fu, X. B. Zhang and W. Tan, *Angew. Chem.*, 2016, **55**, 5477–5482.
108 Z. Liu, S. Zhang, H. Lin, M. Zhao, H. Yao, L. Zhang, W. Peng and Y. Chen, *Biomaterials*, 2018, **155**, 54–63.
109 H. Fan, Z. Zhao, G. Yan, X. Zhang, C. Yang, H. Meng, Z. Chen, H. Liu and W. Tan, *Angew. Chem.*, 2015, **54**, 4801–4805.

